THE JOURNAL OF PHYSICAL CHEMISTRY Letters

pubs.acs.org/JPCL

Perspective

Photoinduced Dynamics of Charge Carriers in Metal Halide Perovskites from an Atomistic Perspective

Lu Qiao, Wei-Hai Fang, Run Long,* and Oleg V. Prezhdo

Cite This: *J. Phys. Chem. Lett.* 2020, 11, 7066−7082

Read Online

ACCESS | Metrics & More | Article Recommendations | Supporting Information

ABSTRACT: Perovskite solar cells have attracted intense attention over the past decade because of their low cost, abundant raw materials, and rapidly growing power conversion efficiency (PCE). However, nonradiative charge carrier losses still constitute a major factor limiting the PCE to well below the Shockley−Queisser limit. This Perspective summarizes recent atomistic quantum dynamics studies on the photoinduced excited-state processes in metal halide perovskites (MHPs), including both hybrid organic−inorganic and all-inorganic MHPs and three- and two-dimensional MHPs. The simulations, performed using a combination of time-domain *ab initio* density functional theory and nonadiabatic molecular dynamics, allow emphasis on various intrinsic and extrinsic features, such as components, structure, dimensionality and interface engineering, control and exposure to various environmental factors, defects, surfaces, and their passivation. The detailed atomistic simulations advance our understanding of electron−vibrational dynamics in MHPs and provide valuable guidelines for enhancing the performance of perovskite solar cells.

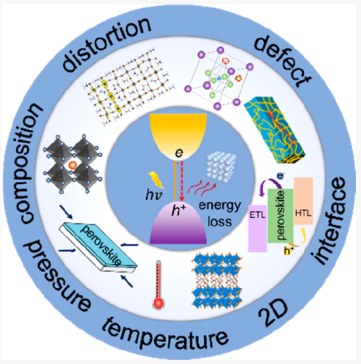

Metal halide perovskites (MHPs) receive remarkable attention in solar energy and optoelectronics[1−4] because of their excellent optoelectronic properties, including high absorption coefficients,[5] large charge diffusion lengths,[6,7] long charge carriers lifetimes,[8−11] and suitable bandgaps that can be easily tuned by alloying via a variety of cations and anions.[12−15] These advantages have further extended the applications to other areas, such as photodetectors[16] and light-emitting diodes.[17,18] Since the first utilization of $CH_3NH_3PbI_3$ (MA = $CH_3NH_3^+$) as a light absorber in 2009,[19] the power conversion efficiency (PCE) of perovskite solar cells has grown rapidly from 3.8%[19] to 25.2%[20] within a decade. However, this record value still lags behind the Shockley−Queisser theoretical limit[21] of a single p−n junction solar cell because of nonradiative charge and energy losses.

In general, electron−vibrational interactions constitute the major source for nonradiative channels with scattering of electrons by simultaneous creation or annihilation of phonons arising from the electronic response to nuclear vibrations.[22] The presence of defects in bulk perovskites or at grain boundaries (GBs) typically accelerate nonradiative processes.[23] Auger-type recombination becomes important when the carrier concentration is high. Auger recombination of an electron and a hole is associated with energy transfer to another charge carrier, followed by the carrier relaxation via phonons and generation of heat.[24] On the one hand, nonradiative losses limit open-circuit voltage and the fill factor of solar cells, hindering further PCE improvements.[23] On the other hand, nonradiative recombination centers, such as point defects, promote degradation of perovskite materials and devices, inhibiting their longevity and commercial development.[25] Therefore, tremendous experimental efforts have been dedicated to eliminating defects and reducing nonradiative energy losses[26−28] by increasing grain size and crystallinity[27] and passivating defects.[28] A large number of ultrafast time-resolved spectroscopy experiments followed the synthetic efforts, generating enormous amounts of data,[29−34] and motivating time-domain atomistic studies aimed at exploring the complex electron−vibrational dynamics with the emphasis of a variety of realistic factors. The present Perspective summarizes the recent key findings obtained in our group on the phonon-assisted charge separation, trapping, and recombination in three- and two-dimensional (3D and 2D) hybrid organic−inorganic and all-inorganic perovskites, and provides important insights for design of high-performance perovskite-based photovoltaic and optoelectronic devices by optimizing photoinduced charge separation and reducing nonradiative charge and energy losses.

The mixed quantum-classical nonadiabatic (NA) molecular dynamics (MD) methodologies[35−43] developed in our group and implemented within the time-dependent (TD) Kohn−Sham (KS) representation of density functional theory (DFT)[44] provide robust tools for modeling nonequilibrium quantum dynamics in condensed phase and nanoscale

Received: May 31, 2020
Accepted: July 31, 2020
Published: July 31, 2020

https://dx.doi.org/10.1021/acs.jpclett.0c01687
J. Phys. Chem. Lett. 2020, 11, 7066−7082

Ab initio quantum dynamics simulations combining nonadiabatic molecular dynamics with time-dependent density functional theory provide a unique tool for modeling far-from-equilibrium evolution of coupled vibrational, electronic, and spin degrees of freedom in nanoscale and condensed matter systems.

materials at the atomistic level of detail and for investigating photoinitiated evolution of coupled charges and vibrations in MHPs. The lighter and faster electrons are treated quantum mechanically, while the heavier and slower nuclei are described semiclassically. To save computational cost, the electronic dynamics are calculated under the classical path approximation (CPA).[45] The CPA assumes that the nuclear dynamics are steered by thermal kinetic energy and are weakly affected by the electronic dynamics. In practical computations, the nuclear trajectories are obtained by performing adiabatic MD simulations, and the electronic wave function or density matrix is propagated by solving the time-dependent Schrodinger or Liouville−von Neumanm equation with the predetermined time-dependent nuclear Hamiltonian. Transitions between electronic states are included in such simulations explicitly. Quantum nuclear effects are captured by incorporating decoherence effects using the decoherence induced surface hopping (DISH) algorithm,[37] summarized in the Supporting Information. Decoherence is a time-domain analogue of the Franck−Condon and Huang−Rhys factors. It strongly influences rates of transitions across large energy gaps encountered during charge trapping and recombination.

DFT provides an adequate and efficient description of electronic properties of MHPs; and therefore, the evolution of the electronic subsystem is described by real-time time-dependent DFT (TD-DFT) in the KS framework.[44] The electron density at time t is expressed by the sum of the densities of the time-dependent occupied single-electron KS orbitals:[46]

$$\rho(\mathbf{r}, t) = \sum_{i=1}^{N_e} |\varphi_i(\mathbf{r}, t)|^2 \tag{1}$$

Applying the time-dependent variational principle to the electron density gives a set of single-particle equations for the KS orbital evolution:[46,47]

$$i\hbar \frac{\partial \varphi_i(\mathbf{r}, t)}{\partial t} = H(\mathbf{r}, \mathbf{R}, t)\varphi_i(\mathbf{r}, t) \tag{2}$$

The equations are coupled because the DFT Hamiltonian H depends on the overall electron density. The electron−vibrational interactions enter the Hamiltonian H through the external potential created by the nuclei. Expansion of the time-dependent single-electron orbitals in eq 2 in the adiabatic KS basis[33] leads to following equations:

$$\varphi_i(\mathbf{r}, t) = \sum_{i=1}^{N_e} c_i(t)|\tilde{\varphi}_i(\mathbf{r}, \mathbf{R}(t))\rangle \tag{3}$$

Inserting eq 3 into eq 2 gives the equation describing the evolution of the expansion coefficients:

$$i\hbar \frac{\partial}{\partial t} c_j(t) = \sum_i c_i(t)(\varepsilon_i \delta_{ji} + \mathbf{d}_{ji}\cdot\dot{\mathbf{R}}) \tag{4}$$

where ε_i is the energy associated with the adiabatic KS orbital i and $\mathbf{d}_{ji}\cdot\dot{\mathbf{R}}$ is the NA coupling between orbitals i and j, computed numerically as the overlap of KS orbitals i and j at sequential time steps:[48,49]

$$\begin{aligned}\mathbf{d}_{ji}\cdot\dot{\mathbf{R}} &= -i\hbar\langle\tilde{\varphi}_j(\mathbf{r}, \mathbf{R}(t))|\nabla_R|\tilde{\varphi}_i(\mathbf{r}, \mathbf{R}(t))\rangle\cdot\frac{d\mathbf{R}}{dt} \\ &= -i\hbar\left\langle \tilde{\varphi}_j(\mathbf{r}, \mathbf{R}(t))\left|\frac{\partial}{\partial t}\right|\tilde{\varphi}_i(\mathbf{r}, \mathbf{R}(t))\right\rangle \\ &\approx -\frac{i\hbar}{2\Delta t}(\langle\varphi_j(t)|\varphi_i(t+\Delta t)\rangle - \langle\varphi_j(t+\Delta t)|\varphi_i(t)\rangle)\end{aligned} \tag{5}$$

The corresponding many-particle equations are given in refs 50 and 51.

In order to describe phonon-induced loss of coherence in the electronic subsystem, the decoherence time is estimated as the pure-dephasing time of the optical response theory.[52] The pure-dephasing time is calculated by the second-order cumulant approximation.[52] The phonon-induced fluctuation of the energy gap between states i and j, $\Delta E_{ij}(t)$, is obtained from the MD trajectory. Then, the energy gap autocorrelation function (ACF) is computed

$$C_{ij}(t) = \frac{\langle \Delta E_{ij}(t)\Delta E_{ij}(0)\rangle_T}{\langle \Delta E_{ij}{}^2(0)\rangle_T} = \frac{C_{un}(t)}{\langle \Delta E_{ij}{}^2(0)\rangle_T} \tag{6}$$

$C_{ij}(t)$ and $C_{un}(t)$ are the normalized and unnormalized ACFs, respectively. The initial value of unnormalized ACF represents the square of the energy gap fluctuation. A large energy gap fluctuation and a rapid ACF decay favor fast dephasing.[50,53]

The pure-dephasing function is calculated by double integration and exponentiation of the unnormalized ACF[52]

$$D_{cumu}(t) = \exp[-g(t)] \tag{7}$$

$$g(t) = \int_0^t d\tau_1 \int_0^{\tau_1} d\tau_2 C_{un}(\tau_2) \tag{8}$$

Fitting eq 7 to a Gaussian gives the pure-dephasing/decoherence time. Computing Fourier transform of the ACF gives the spectral density

$$I(\omega) = \left| \frac{1}{\sqrt{2\pi}} \int_{-\infty}^{\infty} dt e^{-i\omega t} C(t) \right|^2 \tag{9}$$

Also known as the influence spectrum, it characterizes phonon modes that couple to the electronic degrees of freedom and participate in elastic and inelastic electron−vibrational scattering.

The present Perspective summarizes *ab initio* TD-DFT/NAMD studies of phonon-assisted charge separation, trapping, and recombination dynamics in a broad range of perovskites, including 3D hybrid organic−inorganic and all-inorganic MHPs, as well as 2D MHPs. The studies are performed in direct connection with time-resolved experiments and provide microscopic mechanisms for a variety of dynamic processes by considering structure and composition engineering; environmental effects, such as temperature, pressure, and exposure to

https://dx.doi.org/10.1021/acs.jpclett.0c01687
J. Phys. Chem. Lett. 2020, 11, 7066−7082

air and humidity; point and boundary defects and their passivation; surfaces; interfaces; *etc.*

The versatile chemical and structural space of perovskites allows for component engineering aimed at optimizing structural stability, optical properties, and charge carrier dynamics.

Ion Composition Control of Nonradiative Electron−Hole Recombination. Perovskites have the general formula ABX_3 (Figure 1a), where A is a monovalent cation, such as

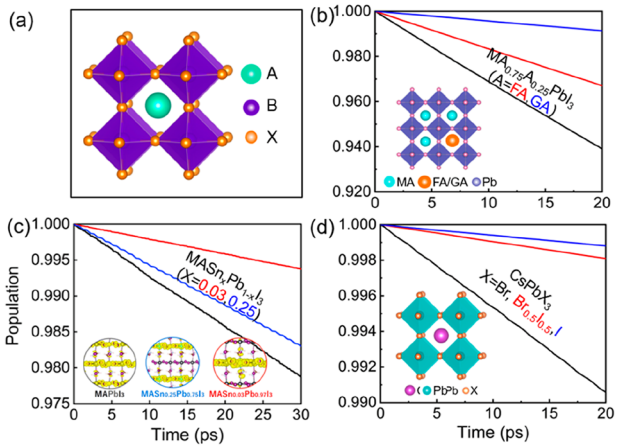

Figure 1. (a) ABX_3 perovskite geometry. Ion alloying affects nonradiative electron−hole recombination in (b) $MAPbI_3$, $MA_{0.75}A_{0.25}PbI_3$ (A= FA, GA), (c) $MASn_xPb_{1-x}I_3$ (x = 0.03 and 0.25), and (d) $CsPbBr_{3-x}I_x$ (x = 0, 1.5, and 3) QDs. The insets in panels b and d present schematics of simulation cells, and the inset in panel c is the VBM charge density. Sn doping induces a significant hole localization, especially in $MASn_{0.03}Pb_{0.97}I_3$. Adapted from refs 71, 74, and 75. Copyright 2018 and 2019 American Chemical Society.

$CH(NH_2)_2^+$ or Cs^+; B is a divalent metal cation, such as Pb^{2+} or Sn^{2+}; and X is a halide anion, such as Cl^-, Br^-, or I^-.[54] The B and X ions form BX_6^{4-} octahedra, and A occupies the cavity formed by four BX_6^{4-} octahedra.[55] The crystallographic stability and structure can be characterized by the tolerance factor t,[56] which can be expressed as $t = (r_A + r_X)/[\sqrt{2}(r_B + r_X)]$. Typically, $0.81 < t < 1.11$ is required to achieve a stable perovskites structure.[56]

Component engineering plays an important role in determining structural stability and optical properties of perovskites.[57−62] It can be realized by alloying foreign ions with the host A, B, and X ions. The traditional $MAPbI_3$ suffers from instability under light irradiation, humidity, and heat, in particular because of the A-site organic MA ions.[63] Partial replacement of smaller MA (methylamine) with larger FA (formamidinium) can not only enhance perovskite stability by increasing the tolerance factor t to 0.88 from 0.83 in the pristine $MAPbI_3$[56] but also extend the absorption edge to the near-infrared region of the solar spectrum by decreasing the bandgap.[57] Importantly, the exited-state lifetime is prolonged in FA-doped $MAPbI_3$, even though the organic ions contribute to neither the conduction band minimum (CBM) nor the valence band maximum (VBM).[64] The charge carrier lifetimes are extended further when $MAPbI_3$ is doped with an even larger GA (guanidinium).[59]

In order to reduce the toxicity of lead atoms and decrease the bandgap of $MAPbI_3$, one can employ partial alloying of alkaline earth[65] and transition metals[66] into the B-site occupied by Pb ions, simultaneously achieving both goals. At the same time, isoelectronic substitution of Pb in $MAPbI_3$ with Sn or Ge has been attempted experimentally. However, the radius of Ge is too small to form stable octahedra after doping into $MAPbI_3$.[67] Alternatively, Sn doping not only offers superior properties, such as high hole mobility[29] and lower bandgap,[62] but also extends charge carrier lifetimes. In general, smaller bandgap correlates with larger NA coupling and faster nonradiative electron−hole recombination. As a consequence, the observation of the prolonged excited-state lifetime remains unexplained.

The stability of all-inorganic perovskites is significantly enhanced compared to the hybrid perovskites. The X-site halogen anions occupy the six vertices of the octahedral BX_6 in perovskites, and the B-site Cs^+ ions occupy the cavity of the BX_6 octahedra. However, the smaller Cs^+ cannot support the BX_6 octahedra perfectly, such that all-inorganic $CsPbX_3$ forms a nonideal cubic phase or quantum dots (QDs). Homologous substitution of iodine with chlorine or bromine is easy to realize experimentally to obtain tunable bandgap, enhanced carrier diffusion length, and extended carrier lifetime.[60,61] The carrier diffusion length in the $CsPbI_3$ perovskite is on the order of ∼100 nm under solar illumination.[68] The replacement of larger iodine atoms with smaller bromines can increase the diffusion length by 2 orders of magnitude to 9.2 μm.[69] Interestingly, the charge carrier lifetimes of $CsPbX_3$ QDs increase dramatically after changing the halide of the precursors from Br to I. However, the underlying mechanism is not clear.[70]

NAMD simulated nonradiative electron−hole recombination time scales increase from pristine $MAPbI_3$ to FA-doped $MAPbI_3$ to GA-doped $MAPbI_3$ (Figure 1b).[71] The replacement of MA with the larger FA and GA cations does not bring significant changes in the bandgap and the charge densities of the band edge states. However, the substitution reduces the NA coupling by increasing the stiffness of the inorganic Pb−I sublattice, which is reflected in the standard deviations of positions of the Pb and I atoms summarized in Table 1.

Table 1. Standard Deviations (Å) in Positions of the Pb and I Atoms in $MAPbI_3$, $MA_{0.75}FA_{0.25}PbI_3$, and $MA_{0.75}GA_{0.25}PbI_3$

system	$MAPbI_3$	$MA_{0.75}FA_{0.25}PbI_3$	$MA_{0.75}GA_{0.25}PbI_3$
Pb	0.537	0.492	0.452
I	0.768	0.602	0.523

Smaller standard deviations imply suppressed atomic motions, leading to smaller NA coupling, because the nuclear velocity, $d\mathbf{R}/dt$, enters the coupling matrix element (eq 5). As a result, the NA coupling decreases in the sequence MA > FA > GA, as the ionic radius of the organic cation increases, rationalizing the observed order of the electron−hole recombination times.[72,73]

Substituting Sn into $MAPbI_3$ at doping concentration leads to interesting charge localization.[74] The simulations show that Sn dopants at low and high doping concentrations form small and large hole polaron-like states in $MAPbI_3$, respectively. The

https://dx.doi.org/10.1021/acs.jpclett.0c01687
J. Phys. Chem. Lett. 2020, 11, 7066−7082

Sn dopant induces distortion of the $[SnI_6]^{4-}$ octahedra by shortening the Sn−I bond length and contracting the I−Sn−I angles, leading to significant hole localization around the Sn atoms, as shown in the inset of Figure 1c. As a result, the overlap between the electron and hole wave functions is reduced, and thus, the NA coupling decreases relative to pristine $MAPbI_3$, rationalizing the changes in the nonradiative electron−hole recombination time scales at low and high doping levels.[74]

Primarily driven by low-frequency Pb−X vibrations below 100 cm^{-1}, charge recombination in $CsPbX_3$ QDs shows strong dependence on X. Replacing half of the bromines with iodines in a $CsPbBr_3$ QD reduces the nonradiative electron−hole recombination rate by a factor of 5, while complete replacement reduces the rate by a factor of 8 (Figure 1d).[75] The recombination rate decreases as lighter bromines are replaced with heavier iodines because the NA coupling is reduced because of the decreased overlap of the electron and hole wave functions and the reduced nuclear velocity. All of the obtained electron−hole recombination time scales agree well with experiments.

The examples considered above demonstrate that a rational choice of alloying ions can suppress nonradiative charge recombination and enhance the photon-to-electron conversion efficiencies in perovskite solar cells.

Distortions of the inorganic lattice and reorientation of organic cations have a significant influence on localization of charge carriers, their interactions, and dynamics. Such phenomena do not arise with traditional inorganic semiconductors that are more rigid.

Charge Separation and Reduced Charge Recombination Due to Reorientation of MA Cations. MA ions occupy the cavities formed by the $[BX_6]^{4-}$ octahedra that share common vertices in $MAPbI_3$.[55] These cavities are sufficiently large to allow the organic MA ions to rotate at ambient temperature. Because the MA ions have an asymmetric electron density distribution and carry dipole moments, they serve as a medium to modulate the electrostatic landscape inside the perovskite structure.[76−79] Simultaneously, the Pb−I inorganic sublattice interacts with the MA ions via short-range steric forces and distorts subject to the MA rearrangement. Experiments reported that both effects can facilitate an efficient separation of photogenerated electron−hole pairs, because both an ordered rearrangement of the dipolar MA ions[80] and distortion of the inorganic octahedra[81] can form nanoscale ferroelectricity domains. The electric field[82] formed in the domains is capable of driving the electrons and holes in opposite directions, improving charge collection, notably reducing nonradiative electron−hole recombination, and enhancing the PCE of solar cells.[82]

In order to explore the atomistic mechanism underlying the extended charge carrier lifetimes and enhanced device performance, we created the ferroelectric (ferro) system containing two domains based on the pristine $MAPbI_3$ supercell (Figure 2a) by aligning the MA ions in the opposite

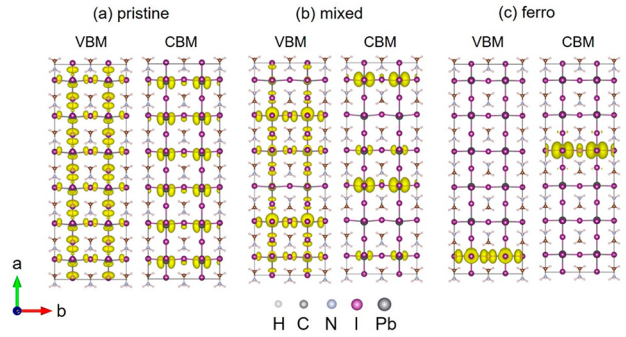

Figure 2. Charge densities of VBM and CBM in (a) pristine $MAPbI_3$, (b) *mixed*, and (c) *ferro* systems. The opposite direction of polar C−N and N−C bonds leads to formation of ferroelectric domains in the *ferro* system, facilitating charge separation and reducing the NA coupling. The extent of charge separation decreases in the *mixed* system. Adapted from ref 83. Copyright 2019 American Chemical Society.

directions (Figure 2c).[83] The mixed system is obtained by rotating the two rows of organic cations by 180° (Figure 2b). By performing NAMD simulations, we demonstrated that the nonradiative electron−hole recombination rates decrease from the pristine $MAPbI_3$ to the mixed system to the ferro system. This is primarily because the ferroelectric alignment of the polar C−N bonds in the ferro system promotes charge localization and separation, decreasing the NA coupling by over a factor of 2 compared to the pristine system (Figure 3).

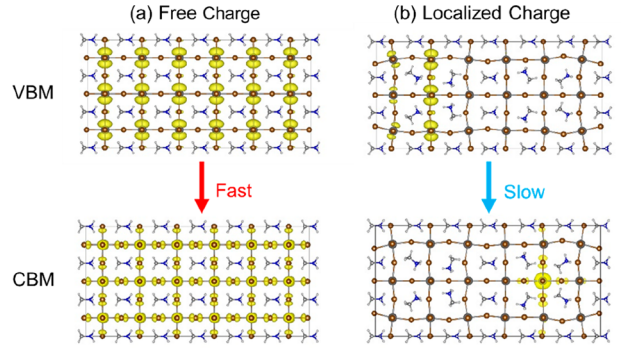

Figure 3. Charge densities of VBM and CBM in $MAPbBr_3$ of (a) higher-bandgap and (b) lower-bandgap structures. The orbitals in the lower gap structure are strongly localized, forming a charge-separated state and slowing nonradiative electron−hole recombination. Stronger orbital delocalization in the higher-bandgap structure results in larger NA coupling and faster nonradiative charge recombination, rationalizing hot fluorescence. Adapted from ref 87. Copyright 2017 American Chemical Society.

This effect enhances the motions of organic and inorganic components and shortens the pure-dephasing time. The two factors compete successfully with the hundreds of millielectronvolt bandgap reduction caused by the enhanced I(5p)−Pb(6s) orbital antibonding interaction due to octahedral distortion pushing the VBM up. The nonradiative electron−hole recombination is reduced by over a factor of 3. The mixed system falls between pristine $MAPbI_3$ and the ferro system, because the NA coupling, pure-dephasing time, and bandgap fall between the values in the other two systems.

In addition to creating the ferroelectric domains, rearrangement of the organic cations in hybrid organic−inorganic

https://dx.doi.org/10.1021/acs.jpclett.0c01687
J. Phys. Chem. Lett. 2020, 11, 7066−7082

perovskites can lead to formation of large polarons spanning many unit cells.[84−86] The formation of large polarons may protect charge carriers, because organic cations screen electron−hole Coulomb interactions and reduce recombination.[76] In addition, polaron formation can rationalize hot luminescence lasting over 100 ps in hybrid organic−inorganic perovskites.[30] In contrast, rotations and other small-amplitude motions of isotropic Cs^+ cations inside the inorganic cage of all-inorganic perovskites are not sufficient to produce hot fluorescence. It has been argued that hot fluorescence in $MAPbBr_3$ lasting over 100 ps originates from slow relaxation of hot electrons within the conduction band. However, this view conflicts with the well-accepted concept that hot carriers relax within only several picoseconds or even hundreds of femtoseconds in bands of condensed-phase materials because of involvement of dense manifolds of electronic states within the band. Bearing this in mind, we proposed that the hot and cold fluorescence in $MAPbBr_3$ can originate from chromophores with different geometric structures and that rearrangement of the organic cations provides one possible example of such different structures. The lower- and higher-bandgap structures correlate with longer and shorter carrier lifetimes, corresponding to the normal and hot fluorescence. To mimic polarons, we focused on $MAPbBr_3$ and rotated half of the MA cations from (x, y, z) to $(-x, y, -z)$ to form the lower-bandgap structure.[87] We changed the MA orientation only in the x-direction from (x, y, z) to $(-x, y, z)$ and obtained the higher-bandgap structure. The higher and lower-bandgap structures, shown in Figure 3a,b, produced delocalized and localized charges. The bandgaps differ by 0.3 eV in the two structure, agreeing well with the experimentally reported difference in the hot and cold fluorescence energies.[30] The bandgap difference arises because formation of polarons leads to electron and hole localization, stabilizes electron and hole, and lowers their energies and the energy gap between them. Compared to the structure with delocalized charges and large bandgap (Figure 3a), the VBM and CBM are localized spatially in different positions in the lower-bandgap structure (Figure 3b). The reduced electron−hole overlap decreases the NA coupling by over a factor of 2, compared to the higher-bandgap structure. The decoherence times of the two systems are almost identical and thus have no influence on the difference in the nonradiative electron−hole recombination time scales. The smaller NA coupling due to electron and hole localization in the lower-bandgap structure leads to a longer nonradiative recombination time, demonstrating that regular, low-energy fluorescence can arise from emission of recombining electron and hole polarons. Alternatively, the shorter-lived high-energy fluorescence can arise from emission of delocalized charge carriers. The study provides a feasible explanation, at the atomistic level, of the unusual hot luminescence phenomenon observed in the experiment.[30]

Shortly after, Miyata et al. reported the first time-domain study of formation of large polarons in the all-inorganic $CsPbBr_3$.[88] Because all-inorganic perovskites contain isotropic Cs^+ cations, whose motions alone cannot form long-range electric structures, large polarons in $CsPbBr_3$ are associated with deformation of the inorganic lattice upon photoexcitation. Similarly to hybrid perovskites, large polarons screen charge carriers and suppress carrier−carrier scattering in all-inorganic perovskites. DFT calculations further demonstrated that coupled stretching and bending motions of the inorganic framework play key roles in the large polaron formation.[88] However, a debate remains regarding localization of electrons and holes between theoretical and experimental works.[88,89] On the theoretical side, Miyata et al. have argued that both electron and hole polarons are delocalized.[88] On the experimental side, however, Chergui and coauthors have shown that photoexcitation leads to a localized hole polaron and a delocalized electron polaron based on time-resolved X-ray near-edge adsorption spectroscopy.[89] Such separation of electrons and holes extends the charge carrier lifetime over 100 ns. By distorting the inorganic Pb−Br sublattice, we demonstrated that indeed $CsPbBr_3$ can form a localized hole polaron and a delocalized electron polaron.[90] The overlap of electron and hole wave functions decreases, and the NA coupling reduces by over a factor of 5 compared to pristine $CsPbBr_3$. At the same time, the deformation of the inorganic sublattice restricts motions of Br and Pb atoms, increasing the decoherence time 2-fold relative to the pristine system. As a result, polaron formation inhibits notable electron−hole recombination by extending the excited-state lifetime 1 order of magnitude relative to pristine $CsPbBr_3$.[90]

Given the NAMD simulations for both hybrid organic−inorganic and all-inorganic perovskites, we suggest that deformation and distortion of the inorganic lattice constitutes the main atomistic mechanism for polaron formation, with rotation of organic cations playing an additional role. Polaron formation separates electrons and holes in different spatial locations and reduces nonradiative electron−hole recombination.

Although perovskites are much more defect-tolerant than many other semiconductors, because of lattice softness and electronic properties of Pb, defects still constitute a major source of charge and energy losses, which can be reduced by passivation.

Suppression of Electron−Hole Recombination by Defect Passivation. Advanced techniques of low-temperature solution synthesis of perovskite films provide improved control over film quality compared to high-temperature synthesis.[91,92] Nevertheless, even the best films still suffer from stoichiometry deviations and improper bonding during crystallization, unintentionally giving rise to defects, such as point defects or large GBs that may form midgap trap states, impending charge carrier transport and serving as nonradiative recombination centers.[93] Because ionic Pb−I (Br) bonds are relatively weak, MHPs have high defect tolerance, with many defects having only minor influence on nonradiative charge and energy losses. In general, shallow trap states positioned energetically close to valence and conduction bands only restrict efficient movement of free charges through trapping and detrapping processes. In contrast, deep trap states capture electrons and holes, which cannot escape by thermal activation and hence will be annihilated with oppositely charged carriers through nonradiative recombination.[92] The latter case is detrimental for charge extraction and limits carrier diffusion lengths, and therefore, it should be strongly avoided. A great number of experiments have been dedicated to this end, resulting in

https://dx.doi.org/10.1021/acs.jpclett.0c01687
J. Phys. Chem. Lett. 2020, 11, 7066−7082

extensive efforts to passivate various defects by Lewis acids[94] and bases,[95] polymers,[96] alkali metals,[31,97,98] and even oxygen[75] and water,[99,100] even though water and oxygen undermine perovskite chemical stability.

It is believed that iodine interstitial (I_i) constitutes a major defect in $MAPbI_3$. It not only causes nonradiative charge and energy losses but also accelerates perovskite decomposition[101] and causes the current−voltage hysteresis.[102] Experimental data have provided controversial conclusions regarding the influence of the iodine interstitial defect on the excited-state lifetimes, including both positive and negative effects.[103,104] DFT calculations have shown that the different oxidation states (0, −1, +1) of iodine interstitial have significant influence on the electronic properties of $MAPbI_3$. By performing NAMD simulations, we showed that the neutral iodine interstitial (I_i) accelerates nonradiative electron−hole recombination, while both the negatively (I_i^{-1}) and positively (I_i^{+1}) charged iodine interstitials slow down the recombination compared to pristine $MAPbI_3$, but by different mechanisms (Figure 4).[105] The

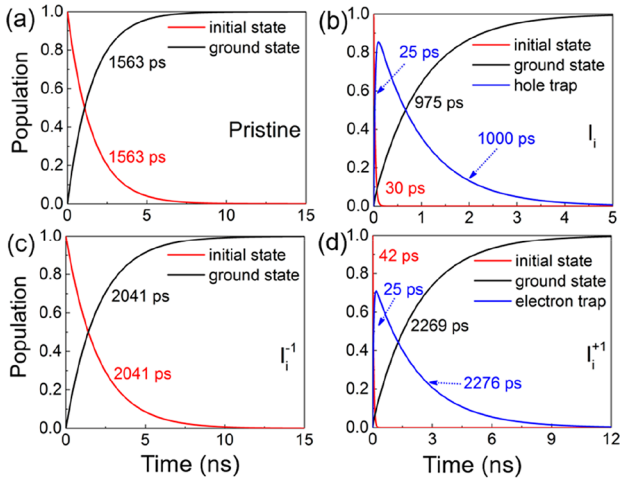

Figure 4. Evolution of populations of the key states for charge trapping and recombination in (a) pristine $MAPbI_3$, (b) I_i, (c) I_i^{-1}, and (d) I_i^{+1} systems. Adapted from ref 105. Copyright 2019 The Royal Society of Chemistry.

neutral I_i creates a half-occupied state that is closer to the VBM than the CBM. Consequently, the state rapidly traps holes, which then recombine with electrons in the CBM (Figure 4b). Charging the defect to I_i^{-1} eliminates the trap state by fully pairing up the electrons. In such a case the electron−hole recombination occurs directly between the CBM and VBM, and the charge carrier lifetime becomes notably longer (Figure 4c). In comparison, I_i^{+1} attracts adjacent iodine anions, leading to formation of an I-trimer, which also creates an electron trap state within the bandgap. The electron is rapidly trapped and then recombines with a VBM hole over 2 ns. However, the positive iodine interstitial is unstable and can readily capture an electron under light illumination and form a more detrimental neutral iodine interstitial.[106] The simulation results show that making iodine interstitial negative suppresses charge recombination. At the same time, iodide ion migration causes a notable current−voltage hysteresis, lowering efficiency of the operation of perovskite solar cells. Interestingly, the negative iodine interstitial can interact with an oxygen molecule and form a stable IO_3^{-1} species, which not only inhibits ion migration in the presence of iodine interstitials but also slows electron−hole recombination further, suggesting that oxygen passivation may have multiple positive effects on perovskite optoelectronic properties.

Experiments demonstrate a factor of 3 increase of photoluminescence quantum yield and extension of photoluminescence lifetime from several to hundreds of nanoseconds when $MAPbI_3$ is exposed to air or oxygen.[107] It has been suggested that the effect arises because of passivation of surface iodine vacancies by adsorbed oxygen and reduction of defect density.[108]

In order to study the atomistic mechanism of the positive effects of oxygen on the optical properties of $MAPbI_3$, we created O_2 and O-doped $MAPbI_3$ containing an iodine vacancy (I_v).[109] Because the system remains neutral overall, removal of an iodine leaves an unsaturated chemical bond with an unpaired electron that gives the vacancy the negative charge. O_2 and O interact with the negatively charged vacancy and form superoxide, O_2^-, and peroxide, $\frac{1}{2}\ O_2^{2-}$. As a result, the superoxide and peroxide species are the most important products of interaction of O_2 with $MAPbI_3$. Shown in Figure 5,

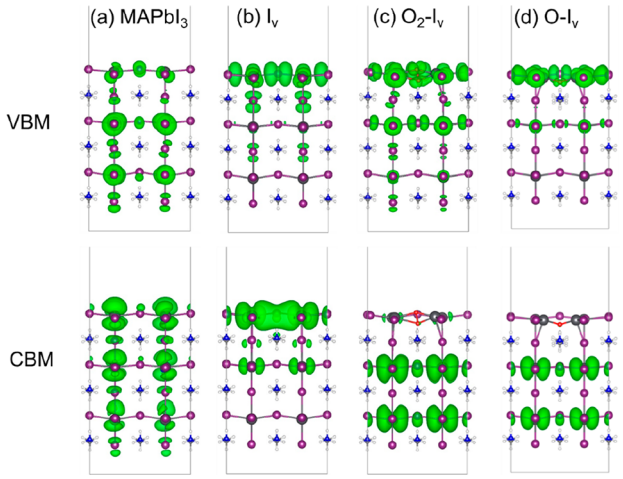

Figure 5. VBM and CBM charge densities in (a) pristine $MAPbI_3$(001) surface, (b) I_v, (c) O_2-doped I_v, and (d) O-doped I_v systems. Although no trap states are created inside the bandgap in the I_v, O_2-doped I_v, and O-doped I_v systems, their VBM and CBM differ significantly. The VBM and CBM overlap in the I_v system and are separated in the O_2-doped I_v and O-doped I_v systems. Adapted from ref 109. Copyright 2019 American Chemical Society.

I_v localizes both electrons and holes at the $MAPbI_3$ surface (Figure 5b), while electrons and holes are distributed over the whole simulation cell in pristine $MAPbI_3$ (Figure 5a). The localization of electrons and holes near the vacancy enhances the NA coupling and accelerates nonradiative electron−hole recombination. In contrast, the superoxide and peroxide species (Figure 5c,d) absorbed at I_v separate electrons and holes, reducing the NA coupling responsible for the charge recombination. At the same time, high-frequency phonon modes created in the superoxide and peroxide systems by light oxygen atoms shorten the decoherence time, while bare I_v softens the phonon modes and retards decoherence. The interplay between the NA coupling and decoherence time leads to the following order of electron−hole recombination time scales: $MAPbI_3 < I_v < O_2^- < O^-$. As a result, the charge carrier lifetime becomes 3−4 times longer in the oxygen passivated systems relative to pristine $MAPbI_3$. Similar

https://dx.doi.org/10.1021/acs.jpclett.0c01687
J. Phys. Chem. Lett. 2020, 11, 7066−7082

phenomena are seen in oxygen-passivated all-inorganic $CsPbBr_3$,[110] in which adsorbed oxygen breaks up lead dimers by forming Pb−O chemical bonds and removes midgap states. The recombination time between the CBM and VBM increases nearly 2-fold compared to pristine $CsPbBr_3$.

Although oxygen treatment can enhance the optical properties of perovskites, oxygen undermines perovskite chemical stability. In order to solve this issue, alkali metals have been used to optimize the performance of perovskite materials and devices.[111,112] Fang et al. reported that lithium can produce free charges by passivating defects to reduce nonradiative energy losses in $MAPbI_3$.[111] Similarity, sodium is able to improve the quality of perovskite films and passivates defects, enhancing the built-in potential and extending carrier lifetimes.[112] Other experiments have demonstrated that potassium, rubidium, and cesium can also reduce defect concentration and extend charge carrier lifetimes.[31,113] Iodine interstitial, one of the main defects in $MAPbI_3$, contains an unpaired electron that can be paired by the single valence electron readily donated by the alkali metals. Motivated by these observations, we investigated passivation of iodine interstitials in $MAPbI_3$ by alkali dopants.[114] The simulations showed that the iodine interstitial formation energy increases significantly in the presence of the alkalis, thereby decreasing defect concentration. If $MAPbI_3$ already contains iodine interstitials, the energies of alkali doping are negative, indicating that the alkalis are easily doped into $MAPbI_3$. Importantly, the doped alkalis eliminate the midgap trap state created by the iodine interstitial. Thus, alkalis increase the number of free carriers capable of generating electrical current by both reducing trap concentration and passivating remaining traps. Importantly, modifying CBM charge density (Figure 6),

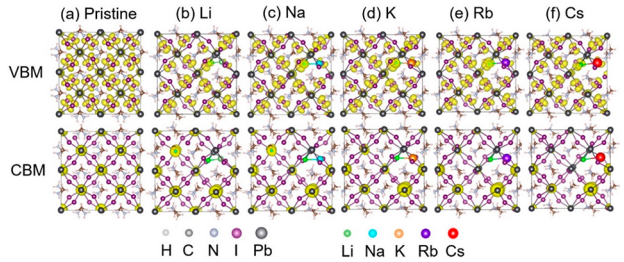

Figure 6. VBM and CBM charge densities in (a) pristine $MAPbI_3$, (b) Li-doped, (c) Na-doped, (d) K-doped, (e) Rb-doped, and (f) Cs-doped iodine interstitial systems. Dopant pushes charge density away from the defect region. Larger alkali atoms create a stronger perturbation. Adapted from ref 114. Copyright 2020 WILEYVCH Verlag GmbH & Co. KGaA, Weinheim.

alkali dopants decrease the NA coupling and decoherence time with increasing alkali ionic radius. Overall, the nonradiative electron−hole recombination time increases in the order I_i < pristine < Li < Na < K < Rb < Cs. Remarkably, the carrier lifetimes in the presence of passivated defects can be up to seven times longer than in pristine $MAPbI_3$. The atomistic time-domain simulations rationalized how alkali doping reduces nonradiative charge carrier losses and improves perovskite solar cell performance.

Debate on the Influence of Grain Boundaries on the Excited-State Lifetimes in $MAPbI_3$. GBs are common defects in polycrystalline perovskite films and can give rise to efficient carrier recombination centers.[115] However, the influence of GBs on charge carrier lifetimes in $MAPbI_3$ and other

Polycrystalline samples contain many grain boundaries which create trap states and cause carrier losses. At the same time, grain boundaries facilitate charge separation, restricting recombination. Annealing can eliminate deep traps and extend carrier lifetimes.

perovskites remains controversial. On the one hand, many experiments have reported that GBs accelerate nonradiative decay and that doping of $MAPbI_3$ GBs by Cl[32] and increasing grain size[116] are effective in prolonging charge carrier lifetimes. On the other hand, opponents have argued that charge recombination happens primarily in non-GB regions of $MAPbI_3$ thin films and that GBs are benign to carrier lifetimes.[117] The different influence of GBs on nonradiative electron−hole recombination and device performance may be ascribed to different types of GBs. We demonstrated this fact by considering $MAPbI_3$ containing Σ5(012) and Σ5(013) GBs and simulating the nonradiative electron−hole recombination.[118,119]

The simulations showed that the Σ5(012) GB accelerates electron−hole recombination, while Cl doping delays the recombination, compared to pristine $MAPbI_3$, Figure 7a.[118] The recombination is accelerated because the Σ5(012) GB creates midgap defect states and enhances the NA coupling. The trap states are created because of unsaturated chemical bonds. The NA coupling is enhanced because electron and hole wave functions are localized around the boundary and because the symmetry breaking at the boundary region relaxes selection rules for electron−phonon coupling and activates additional phonon modes that couple to the electronic subsystem. As a result, charge recombination in the Σ5(012) GB system is 5 times faster than in pristine $MAPbI_3$.

The negative effect of the GB on the charge carrier lifetimes is eliminated by Cl doping. Chlorine atoms replaces iodines in the perovskite structure, and the dopants prefer to accumulate at GBs rather than in bulk, because the energy cost of replacing native atoms with dopants is lower at GBs. The VBM in MHP originates from atomic orbitals of halides. Chlorine is more electronegative than iodine, and therefore, its atomic orbitals are lower in energy and do not contribute to the VBM of Cl-doped $MAPbI_3$. Hence, the whole wave function is pushed away from the Cl-doped GB. Electrons and holes are separated. The overlap of their wave functions and the NA coupling are reduced relative to the undoped GB, and the NA coupling becomes similar to that in the pristine system. At the same time, lighter Cl atoms introduce higher-frequency vibrations and accelerate quantum coherence loss. Both factors compete successfully with the smaller bandgap in the Σ5(012) GB system relative to pristine $MAPbI_3$ and slow down electron−hole recombination. The presence of the Σ5(012) GB in the all-inorganic $CsPbBr_3$ and its passivation by Cl lead to the same conclusions[120] as in $MAPbI_3$.

In contrast, the Σ5(013) GB does not accelerate electron−hole recombination compared to pristine $MAPbI_3$.[119] The relaxed Σ5(013) GB structure exhibits only shallow defect states within 0.1 eV from band edges. The shallow states

https://dx.doi.org/10.1021/acs.jpclett.0c01687
J. Phys. Chem. Lett. 2020, 11, 7066−7082

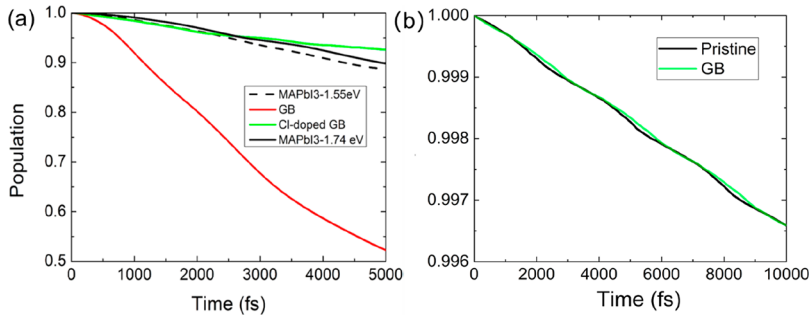

Figure 7. Electron−hole recombination in (a) $MAPbI_3$, Σ5(012) GB, and Cl-doped Σ5 (012) GB and (b) $MAPbI_3$ and Σ5(013) GB. The Σ5(012) GB accelerates charge recombination, while the Σ5(013) GB has little influence on the electron−hole recombination. Adapted from refs 118 and 119. Copyright 2016 and 2019 American Chemical Society.

localize holes and promote electron−hole separation and, therefore, reduce the NA coupling. The charge separation and symmetry breaking allows higher-frequency phonon modes to couple to charges, accelerating the loss of quantum coherence. As a result, the excited-state lifetime in the Σ5(013) GB system remains almost the same as in pristine $MAPbI_3$. On the one hand, GBs help to separate electrons and holes and dissociate photogenerated excitons. On the other hand, GBs do not necessarily accelerate charge recombination. The results show that annealing of polycrystalline $MAPbI_3$ can facilitate GB reconstruction and significantly improve its performance.

Combined together, the results from the Σ5(012) and Σ5(013) GB simulations demonstrate the positive and negative effects of GBs on charge carrier lifetimes and performance of perovskite solar cells and rationalize why different experiments come to different conclusions. The studies also establish and explain the positive effect of Cl doping on the excited-state lifetime. The conclusions about the passivation mechanism can apply to other GBs passivated by various compounds, such as Lewis bases,[95,96] polymers,[81] and water.[100]

Moderate perturbations to the perovskite lattice at elevated temperatures or pressures enhance charge localization, reduce overlap of electron and hole wavefunctions, and slow down electron−hole recombination.

Unusual Dependence of Charge Recombination on Temperature and Pressure. In addition to the intrinsic defects having a strong influence on the optoelectronic properties of perovskites, extrinsic factors, such as humidity,[121] temperature,[122] and pressure,[33] also have remarkable impact on the stability and performance of perovskite solar cells. Our previous work has demonstrated the positive and negative effects of water molecules on the excited-state lifetimes in $MAPbI_3$,[123] and our recent Perspectives has presented the findings.[22,124] Here, we focus on reviewing the influence of temperature and pressure on the nonradiative electron−hole recombination dynamics.

Experiments reported an uncommon temperature dependence of charge carrier lifetimes in $MAPbI_3$, with the lifetimes increasing with temperature.[122,125] The phenomenon is opposite to what is observed in the traditional semiconductors, because high temperature typically gives rise to increased atomic fluctuations and stronger electronic−vibrational interactions. Indeed, atomic fluctuations grow with temperature in $MAPbI_3$ as well. However, the fluctuations give rise to several effects that extend the lifetimes. The fluctuations distort the inorganic Pb−I lattice, increasing localization and separation of electrons and holes, and reducing electron−hole overlap, and correspondingly, the NA coupling (Figure 8a). Enhanced

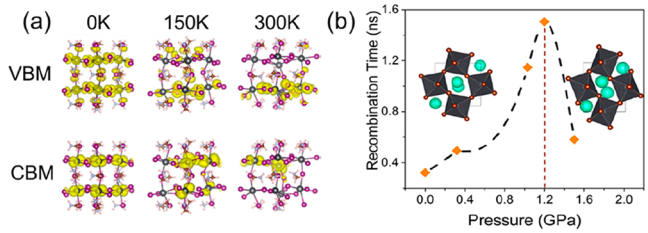

Figure 8. (a) VBM and CBM charge densities of $MAPbI_3$ in tetragonal phase at 0, 150, and 300 K. Charge localization increases as temperature increases because of disorder. (b) Dependence of electron−hole recombination in $CsPbBr_3$ on external pressure. Adapted from refs 126 and 130. Copyright 2018 and 2019 American Chemical Society.

elastic electron−phonon scattering at higher temperatures shorten the quantum coherence time. The reduced NA coupling and shorter coherence slow down the nonradiative relaxation by over a factor of 2 at 300 K compared to 150 K and rationalize the unusual behavior of the carrier lifetimes in $MAPbI_3$ with temperature.[126]

External pressure also influences charge carrier dynamics in both hybrid organic−inorganic perovskites, such as $MAPbI_3$,[127] and all-inorganic perovskites, such as $CsPbBr_3$.[33] Pressure engineering provides a clean method to control device performance, without generating adverse chemical and thermal effects. Previous DFT work[128] proposed that, by bringing atoms closer together, pressure enhances the antibonding interaction between Pb and I atomic orbitals in $MAPbI_3$ and pushes the VBM up on energy. As a result, shallow hole trap states merge into the valence band, and electron−hole recombination is reduced. Experiments reported that application of external pressure to $CsPbBr_3$ can simultaneously narrow the bandgap and increase the carrier lifetime.[33,129] This anticorrelation is surprising because a reduced gap is usually associated with larger NA coupling and faster nonradiative relaxation. By performing NAMD simulations, we rational-

https://dx.doi.org/10.1021/acs.jpclett.0c01687
J. Phys. Chem. Lett. 2020, 11, 7066−7082

ized[130,131] the unusual anticorrelation between the bandgap and the lifetime in $MAPbI_3$ and demonstrated[130] that the nonradiative electron−hole recombination time in $CsPbBr_3$ depends significantly on pressure. Shown in Figure 8b, the recombination time changes as a volcanic plot with increasing pressure. The bandgap of $CsPbBr_3$ changes relatively little for all studied values of pressure and has a minor influence on the excited-state lifetime compared to other factors. The lifetime is governed by interplay between the NA coupling and the decoherence time. Application of pressure distorts perovskite crystal structure and influences atomic motions. Structural disorder leads to charge localization, which typically enhances charge separation and reduces the NA coupling. Pressure-induced perturbation makes atomic motions less harmonic and increases their amplitude, which accelerates loss of coherence but can increase the NA coupling. The longest excited-state lifetime is found for 1.20 GPa, because the NA coupling is smallest at that pressure. Further pressure increase enhances fluctuations of Pb and Br atoms, while having less influence on localization of electron and hole wave functions, thereby increasing the NA coupling.

The *ab initio* NAMD studies provided an atomistic understanding of the unexpected variations in charge carrier lifetimes with temperature and pressure and generated valuable insights into the unusual properties of MHPs.

Tuning interfacial interactions by surface passivation and doping can be used to accelerate charge separation and reduce recombination across interfaces of perovskites with charge extraction and transport materials.

Influence of Interfacial Interactions on Charge Separation and Recombination. In addition to photoexcitation dynamics within perovskites themselves, charge separation and recombination across interfaces between perovskites and charge-transporting materials play important roles in solar cell operation, because charge separation across interfaces constitutes one of the fundamental steps. To be utilized in an efficient solar cell, an interface should be designed to achieve fast charge separation and slow charge recombination. An offset between band energies of the two components forming an interface provides the driving force for the photoinduced interfacial charge transfer, which results in generation of free charge carriers, ultimately leading to conversion of solar energy into electrical or chemical energy. Typically, the faster the charge separation, the slower the recombination, because separated charges cannot meet each other and recombine. Once charges are separated, they can be extracted and collected for power conversion. Furthermore, if charges can separate before relaxing to their lowest energy states in each material, they are less likely to get trapped by defects. Therefore, a rational choice of materials for charge extraction and transport constitutes an important consideration in solar cell design.

Metal oxides, such as TiO_2 and NiO, present popular electron- and hole-transporting materials, respectively, because they possess superior conductivity and stability relative, for example, to organic transporting materials, and have correct band energy alignment with MHPs. It is desirable that the relevant band energy offset between two materials forming an interface for charge extraction is not too large. Otherwise, significant amounts of energy would be lost to heat during the extraction. Thus, the optical bandgap of TiO_2 is 3.2 eV, and its valence band edge is significantly lower than that of $MAPbI_3$, by about 2.1 eV. Such arrangement cannot be used for hole extraction, which requires the valence band edge of the transporting material to be higher than that of perovskite. However, the conduction band edge of TiO_2 is lower than that $MAPbI_3$ and only by 0.4 eV,[132] presenting a favorable situation for electron extraction.[133] NiO is also a wide bandgap (3.6 eV) semiconductor. It makes a good hole extraction and transporting material, because its VBM at −5.2 eV is only slightly above the $MAPbI_3$ VBM at −5.4 eV.[134] Inverted structure perovskite solar cells utilizing NiO as the hole-transporting material exhibit high (21.6%) PCE.[135]

Considering the $MAPbI_3/TiO_2$ system, experiments reported electron transfer from $MAPbI_3$ into TiO_2 to occur over a broad range of time scales, from sub-200 fs to several hundreds of picoseconds.[34,136] Focusing on the faster component, arising from electrons that are already close to the interface, we simulated the electron transfer and electron−hole recombination at a $MAPbI_3/TiO_2$ heterojunction (Figure 9a). The electron transfer is fast, sub-200 fs, because interfacial

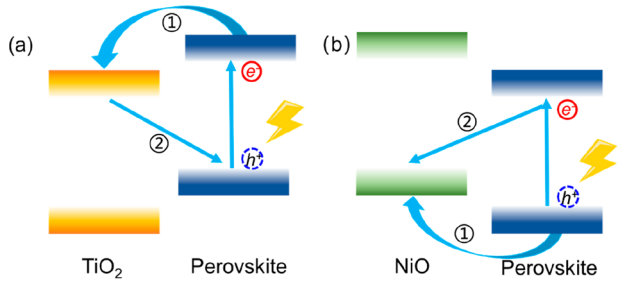

Figure 9. Schematic of photoinduced charge transfer and recombination dynamics between perovskites, and (a) electron and (b) hole transport materials. Photoexcitation promotes an electron from the perovskite valence band to its conduction band. Electrons or holes transfer into the transport materials, ①. Electrons and holes recombine at the interface, ②.

I−Ti bonds provide strong donor and acceptor interactions.[137] The excited state of the heterojunction created by light absorption has a significant charge-transfer character, with a larger fraction of excited electron's density already delocalized onto the TiO_2 acceptor from the $MAPbI_3$ donor. The remaining electron density transfers to TiO_2 by the adiabatic mechanism due to strong covalent donor−acceptor interaction.[138] Following the charge separation, the hole residing in the $MAPbI_3$ VBM recombines with the electron in the TiO_2 CBM on a nanosecond time scale. Partial replacement of I atoms with Cl and Br, or Pb with Sn, influences the nonradiative electron−hole recombination time.[138] In particular, Cl and Br doping extends the carrier lifetime, while Sn doping shortens it. Several considerations rationalize the longer recombination time across the Cl- and Br-doped interfaces. First, the Pb−Cl and Pb−Br bonds are shorter than the Pb−I bond, thus the Cl and Br atoms are farther away from the TiO_2 surface, and the donor−acceptor interaction is weaker. Second, the Cl and Br atoms do not contribute to the $MAPbI_3$ VBM, and therefore, the hole is pushed away from the interface, and the NA coupling is reduced. Third, the lighter dopants

https://dx.doi.org/10.1021/acs.jpclett.0c01687
J. Phys. Chem. Lett. 2020, 11, 7066−7082

introduce higher-frequency vibrations, accelerating quantum decoherence. In contrast, Sn contributes the hole wave function and increases the NA coupling, accelerating the electron−hole recombination. Promoted by low-frequency perovskite and TiO_2 vibrations, the recombination ranges from 0.52 ns in the Sn-doped system to 2 ns in the Cl-doped heterojunction, agreeing well with the experiments.[138]

Subsequently, we investigated hole transfer and electron−hole recombination in a $MAPbI_3$/NiO heterojunction (Figure 9b), considering both low and ambient temperatures.[139] Both processes showed weak temperature dependence, in agreement with the weak temperature dependence of performance of perovskite solar cells observed experimentally.[139] At both higher and lower temperatures, the hole transferred within 100 fs, while hole energy loss to heat took over 200 fs. The relatively long existence of a "hot" hole favors hole transport away from the interface, preventing interfacial electron−hole recombination. Following the charge separation, electron−hole recombination happened on a much longer, nanosecond time scale. The recombination was twice faster at the higher temperature, because of enhanced atomic motions that increased the NA coupling. Compared to electron−hole recombination that occurs between band edge states, hole transfer occurs within a dense manifold of states, in which the NA coupling is already large and changes little with temperature. The balance of fast charge separation and slow recombination across interfaces of MHPs with charge extraction and transporting materials plays an important role in obtaining high-performance solar cells.

Layer thickness in 2D perovskites provides an additional handle on perovskite properties and charge carrier dynamics due to quantum confinement, changes in dielectric environment, high spatial anisotropy, and edge states.

Electron−Hole Recombination in Two-Dimensional Ruddlesden−Popper and Dion−Jacobson Perovskites. Dimensionality provides another handle for tuning perovskite properties. 2D Ruddlesden−Popper (RP) and Dion−Jacobson (DJ) perovskites have emerged as alternatives to the traditional 3D perovskites because of their enhanced moisture resistance, greatly improved optical and thermal stability,[140] small charge effective mass,[141] and large conductivity.[142] The general formulas for RP and DJ perovskites are $A_2A'_{n-1}M_nX_{3n+1}$ and $AA'_{n-1}M_nX_{3n+1}$, respectively. Here, A and A′ are organic cations; M is a metal cation; X is a halogen anion, and n is the number of the inorganic layers inserted between the long organic chains A.[143] The RP phase has two monovalent spacer cations, while DJ perovskites have only one bivalent spacer cation to separate two adjacent inorganic layers. As a typical representative of the RP perovskites, $(BA)_2(MA)_{n-1}Pb_nI_{3n+1}$, BA = $CH_3(CH_2)_3NH_3$, has received intense attention because of its superior optoelectronic properties, stability, and simple crystal structure.[144,145]

Recently, Guo et al. reported that the excited-state lifetime of $(BA)_2(MA)_{n-1}Pb_nI_{3n+1}$ is strongly dependent on the inorganic layer thickness, increasing from 250 ps for n = 1 to a nanosecond for n = 3.[146] The difference was rationalized by the increased dielectric constant and Coulomb screening for n = 3 and, therefore, a reduced electron−hole interaction. Generally, inorganic materials have a larger dielectric constant than organics, and therefore, a relatively thicker inorganic layer increases the screening. However, the Coulomb interaction between electrons and holes is not the only factor determining the charge carrier lifetimes, in particular because charge coupling to phonons constitutes the main recombination mechanism, as opposed to Auger-type scattering of three or more charges that operates only at high carrier densities.

There exist several reasons to be surprised why the n = 3 perovskite exhibits a longer lifetime than the n = 3 perovskite. First, the bandgap for n = 3 is smaller than for n = 1 because of reduced quantum confinement, and a smaller bandgap leads to a larger NA coupling and faster relaxation. Second, the inorganic lattice in the n = 3 perovskite contains a wide range of phonon modes, and therefore, the electron−phonon coupling should be stronger and the electron−phonon relaxation faster. Third, MA cations are embedded into the inorganic lattice of the n = 3 system, while MA is not present at all in the n = 1 perovskite. The light organic MA cations rapidly move inside the lattice, create strong and rapidly varying local electric fields, and interact with charges contributing further to the NA coupling.

By performing NAMD simulations, we demonstrated that the presence of multiple phonon modes in the n = 3 perovskites leads to rapid loss of quantum coherence (Figure 10a).[147] This factor outcompetes the stronger NA coupling and smaller bandgap, extending the excited-state lifetime in $BA_2MAPb_4I_{13}$ to nanoseconds.

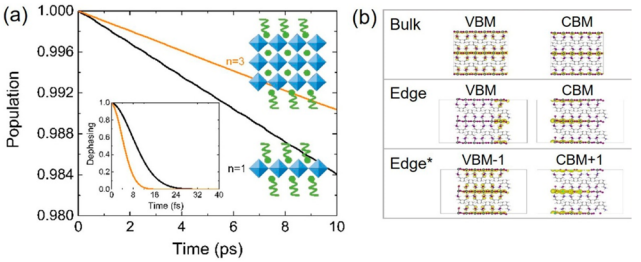

Figure 10. (a) Electron−hole recombination in BA_2PbI_4 and $BA_2MAPb_3I_{10}$. The trilayer perovskite shows a slower decay because of a shorter pure-dephasing time compared to the monolayer perovskite (inset of panel a). (b) Charge densities of VBM and CBM for Bulk and Edge configurations of $(BA)_2PbI_4$, and VBM-1 and CBM+1 for the Edge configuration, marked as Edge*. Charges are delocalized in the Bulk configuration and are localized at the opposite ends in the Edge configuration. The VBM arising from I atoms is more localized than the CBM supported by Pb orbitals in Edge. Adapted from refs 147 and 149. Copyright 2019 American Chemical Society.

In addition to the unusual layer-dependent photoluminescence lifetime, 2D perovskites exhibit important edge effects. It was reported experimentally that edges facilitate exciton dissociation and prolong charge carrier lifetimes.[148] In order to explore the mechanism for these phenomena, we simulated nonradiative electron−hole recombination across the CBM−VBM energy gap in $(BA)_2PbI_4$, including both the fully periodic structure, denoted as Bulk, and the same structure with edges, denoted as Edge, Figure 10b.[149] We also modeled the transition between VBM-1 and CBM+1, denoted as Edge*, in order to represent recombination between electrons and

https://dx.doi.org/10.1021/acs.jpclett.0c01687
J. Phys. Chem. Lett. 2020, 11, 7066−7082

holes localized in the central region of the structure with edges. The simulations showed holes are localized at edges much more than electrons. This is because electrons are supported by Pb atoms that can form isotropic metallic bonds, support multiple oxidation states, and can heal defects associated with unsaturated chemical bonds. In contrast, holes are localized on under-coordinated iodine atoms that are nonmetals and require directional single-valence bonding in order to heal defects, which is more difficult to achieve (Figure 10b). Having studied different types of edge termination, we concluded that charges tend to localize on opposite edges and that the NA coupling is smaller in the Edge than Bulk system. Charge localization at the edges not only promotes exciton dissociation but also reduces overlap of wave functions of electrons and holes and extends their lifetime. In addition, the Edge geometry is less rigid, more anharmonic, and less symmetric, activating additional high-frequency modes, accelerating loss of coherence, and facilitating electron and hole separation even in the central region represented by CBM+1 and VBM-1. This behavior remains true for both Edge and Edge* transitions. The edges reduce the NA coupling and shorten the coherence time, slowing down the nonradiative electron−hole recombination.

DJ perovskite solar cells represent another class of popular photovoltaic devices, whose PCE has increased to 17.9% from the initial 7.32% within only one year.[150−153] The great success motivates substantial efforts focusing on synthesis of high-quality films, exploration of their photophysical properties, and optimization of device performance. Mao et al. reported that the photoluminescence lifetimes in the (3AMP)-$(MA)_{n-1}Pb_nI_{3n+1}$ layered DJ perovskite are over 4 times longer than that in $(4AMP)(MA)_{n-1}Pb_nI_{3n+1}$, where n = 1, 2, 3, 4; 3AMP stands for 3-(aminomethyl) piperidinium, and 4AMP denotes 4-(aminomethyl) piperidinium, regardless of the value of n, even though the 3AMP perovskites have bandgaps smaller than that of the 4AMP perovskite. The mechanism explaining this observation remained largely unclear because the two structures are very similar, and the smaller bandgap should correlate with a shorter carrier lifetime. Focusing on n = 2, our simulations showed that the decoherence times are nearly identical in the two systems and cannot explain the difference in the excited-state lifetimes. A smaller octahedral tilting in $(3AMP)(MA)Pb_2I_7$ leads to a stronger antibonding interaction that determines the VBM energy level. As a result, the VBM is higher in energy and the bandgap is smaller by about 0.15 eV in $(3AMP)(MA)Pb_2I_7$ compared to $(4AMP)(MA)Pb_2I_7$. Importantly, the VBM and CBM charge densities are localized on different parts of the 3AMP system, layers L2/L4 and L1/L3, respectively (Figure 11). The reduced VBM−CBM overlap leads to a smaller NA coupling. In contrast, the VBM of the 4AMP system is delocalized over all inorganic layers, though the CBM remains localized on L1/L3. The overlap of the VBM and CBM wave functions is larger in this case, and the NA coupling is increased by over a factor of 2. The smaller NA coupling, arising from the greater hole localization, serves to slow down nonradiative electron−hole recombination in the 3AMP perovskites.[139]

Our detailed atomistic time-domain studies provide mechanistic understanding of the excited-state dynamics in the RP and DJ 2D halide perovskites, reveal the key influence of localization of charge carriers on their lifetimes, and suggest strategies to design efficient photovoltaic and optoelectronic devices based on layered 2D perovskites.

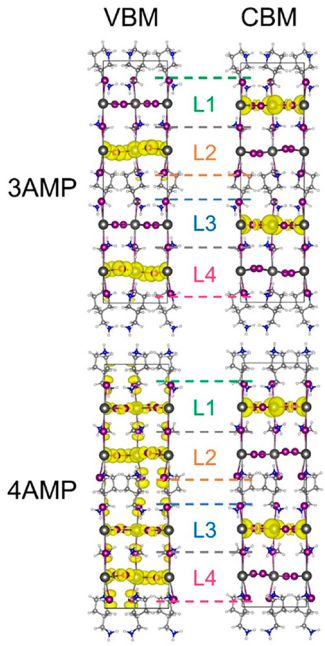

Figure 11. Charge densities of VBM and CBM in $(3AMP)(MA)Pb_2I_7$ and $(4AMP)(MA)Pb_2I_7$. The large overlap between the VBM and CBM in $(4AMP)(MA)Pb_2I_7$ enhances NA coupling and accelerates nonradiative electron−hole recombination. Adapted from ref 139. Copyright 2020 The Royal Society of Chemistry.

Time-domain atomistic simulations of excited-state dynamics in metal halide perovskites provide important insights into the key factors that govern the evolution of optical, electrical, and chemical energy, and help design more efficient perovskite solar cells and other optoelectronic devices.

In summary, hybrid organic−inorganic and all-inorganic perovskites are promising candidates for photovoltaic and optoelectronic applications. Although the recorded PCE of the perovskite solar cells is as high as 25.2%, it is still lower than the Shockley−Queisser limit[21] because of nonradiative charge and energy losses arising from electron−phonon scattering and accelerated by various defects.[25] In this Perspective, we have reviewed the time-domain atomistic simulations of nonradiative charge separation, trapping, and recombination dynamics in 3D and 2D hybrid organic−inorganic and all-inorganic perovskites, mimicking directly time-resolved pump−probe experiments by computing geometry-dependent electron−vibrational coupling and modeling electron−nuclear dynamics explicitly in the time-domain. The simulations provide unique insights into the atomistic mechanisms of the phonon-induced charge dynamics in perovskites with the emphasis on a broad range of factors, involving component, structure, and dimensionality engineering; temperature; pressure; surfaces; interfaces; grain boundaries; defects and their passivation; exposure to radiation, humidity, and oxygen; *etc*.

https://dx.doi.org/10.1021/acs.jpclett.0c01687
J. Phys. Chem. Lett. 2020, 11, 7066−7082

Using the state-of-the-art NAMD and TD-DFT simulation methodologies developed in our group, we demonstrate that an interplay between energy gap, NA coupling, and decoherence time determines charge trapping and recombination dynamics. We show that alloying ions at the A, B, or X sites in hybrid and all-inorganic perovskites can delay electron−hole recombination by several mechanisms. A partial replacement of MA cations with larger cations can enhance lattice stiffness and decrease the NA coupling.[71,75] The replacement of Br with I or Pb with Sn decreases the overlap of electron and hole wave functions,[111,74] leading to a reduction in NA coupling and slowing electron−hole recombination. Rotation of MA cations causes formation of ferroelectric domains or polarons that promote charge separation, reduce NA coupling, and inhibit charge recombination.[83,87] Alternatively, photoexcitation can also lead to slow recombination by localizing holes because of lattice deformation. We demonstrate why and how the oxidation state of the iodine interstitial defects influences charge trapping and recombination and show that negatively charged iodine interstitials contribute to reduction of the recombination in real materials. Interacting with oxygen, interstitial iodine forms stable IO_3^-, which reduces the recombination rate further by decreasing NA coupling and shortening decoherence time. O_2 or O interacting with $MAPbI_3$ containing iodine vacancies form superoxide and peroxide species, which reduce NA coupling by separating electron and hole wave functions, and slow electron−hole recombination relative to the pristine case. However, oxygen undermines the chemical stability of perovskites.[154] Passivation of iodine interstitials by alkali metals can eliminate midgap states and thus extend charge carrier lifetimes.[114] GBs are considered one of the main causes of nonradiative charge carrier losses in perovskites. However, the influence of GBs on the excited-state lifetimes in perovskites is not always negative and depends on GB type, requiring additional investigatio.[118,119] Passivation of GBs with chlorine atoms, which replace intrinsic iodines, pushes holes away from the boundary, decreases electron−hole overlap, reduces NA coupling, accelerates loss of coherence because of both charge separation and introduction of higher-frequency vibrations, and inhibits electron−hole recombination.[118] Higher temperatures enhance atomic fluctuations, cause lattice distortions and charge localization, reduce NA coupling, and accelerate decoherence and, thus, suppress electron−hole recombination compared to lower temperatures.[126] External pressure also distorts the inorganic lattice, causing changes in NA coupling and decoherence time and influencing electron−hole recombination.[130]

Ultrafast electron transfer at $MAPbI_3/TiO_2$ and related junctions is promoted by vibrational motions of both perovskite and TiO_2 and occurs primarily by the adiabatic mechanism because of the presence of strong covalent I−Ti bonds at the interface.[138] Substitution of heavier I with lighter Cl or Br shortens decoherence time and reduces NA coupling, inhibiting charge recombination across the interface. In contrast, replacement of Pb with Sn enhances NA coupling, because Sn is lighter than Pb and contributes to the band edge states, accelerating recombination.[138] Hole transfer and electron−hole recombination at the $MAPbI_3/NiO$ interface show weak temperature dependence,[139] rationalizing why the experimentally reported perovskite solar cell efficiency is independent of temperature.[155] Multiple-layer 2D RP perovskites contain high-frequency vibrations, which facilitate rapid elastic scattering that gives rise to longer-lived excited states compared to the single-layer 2D perovskites.[147] Furthermore, 2D perovskite edges can localize both holes and electrons, especially holes that are supported by nonmetal iodine atoms, facilitating exciton dissociation and favoring long-lived excited states.[149] The different extent of charge localization in DJ perovskites, ascribed to variations in the strength of hydrogen bonding, modulates NA coupling and leads to longer-lived charge carriers in 3AMP compared to 4AMP perovskite.[139]

In addition to the above phenomena, other complex effects contribute to charge carrier dynamics in the perovskites. Spin−orbit interactions facilitated by the heavy Pb atoms induce a direct-to-indirect bandgap transition,[156] suppressing electron−hole recombination, because triplet-to-singlet recombination requires a spin-flip. Auger processes become important at high charge carrier concentrations. Auger recombination is associated with energy exchange between at least three particles, i.e., recombining electron and hole with another particle, followed by electronic energy transfer to heat. In order to optimize the performance of solar cells, it is important to elucidate the interplay of particle−particle and particle−phonon interactions, which can occur on a similar time scale and influence each other.[157] NAMD simulations including complex features beyond point defects of the Frenkel and Schottky types are highly desired, because they are common in perovskites and have significant impact on ion migration and excited-state properties. Future efforts should be devoted to modeling of photoexcitation dynamics in large, realistic systems, which may require development of novel NAMD algorithms and implementations based on tight-binding DFT[158] and machine learning (ML).[159] ML can be used to uncover nontrivial correlations that are hard to anticipate *a priori*.[160] Atomistic quantum dynamics studies have a unique capability to generate valuable knowledge that can provide critical insights for improving the performance of perovskite photovoltaic and optoelectronic devices.

■ ASSOCIATED CONTENT

Supporting Information

The Supporting Information is available free of charge at https://pubs.acs.org/doi/10.1021/acs.jpclett.0c01687.

Decoherence-induced surface-hopping algorithm (PDF)

■ AUTHOR INFORMATION

Corresponding Author

Run Long − *College of Chemistry, Key Laboratory of Theoretical & Computational Photochemistry of Ministry of Education, Beijing Normal University, Beijing 100875, P.R. China;* orcid.org/0000-0003-3912-8899; Email: runlong@bnu.edu.cn

Authors

Lu Qiao − *College of Chemistry, Key Laboratory of Theoretical & Computational Photochemistry of Ministry of Education, Beijing Normal University, Beijing 100875, P.R. China*

Wei-Hai Fang − *College of Chemistry, Key Laboratory of Theoretical & Computational Photochemistry of Ministry of Education, Beijing Normal University, Beijing 100875, P.R. China;* orcid.org/0000-0002-1668-465X

Oleg V. Prezhdo − *Department of Chemistry, University of Southern California, Los Angeles, California 90089, United States;* orcid.org/0000-0002-5140-7500

https://dx.doi.org/10.1021/acs.jpclett.0c01687
J. Phys. Chem. Lett. 2020, 11, 7066−7082

Complete contact information is available at:
https://pubs.acs.org/10.1021/acs.jpclett.0c01687

Notes

The authors declare no competing financial interest.

Biographies

Lu Qiao received her Bachelor degree in Chemistry from the Hebei Normal University and is currently a third-year Ph.D. student under the supervision of Professor Run Long in physical chemistry at the Beijing Normal University. Her research focuses on simulation of photoexcitation charge and energy dynamics in metal halide perovskites.

Wei-Hai Fang is a Professor of Chemistry at the Beijing Normal University and a member of Chinese Academy of Sciences. His research interests range from fundamental aspects of theoretical photochemistry and photophysics to excitation dynamics in molecular systems.

Run Long obtained his Ph.D. in atomic and molecular physics from Shandong University and is currently a Professor of Chemistry at the Beijing Normal University. Dr. Long's research interests are focused on excitation dynamics in nanoscale systems, in particular energy- and charge-transfer dynamics in condensed phase and at interfaces.

Oleg V. Prezhdo is a Professor of Chemistry, and Physics and Astronomy at the University of Southern California. He is a Fellow of the American Physical Society and Executive Editor for the *Journal of Physical Chemistry Letters*. His research interests range from fundamental aspects of semiclassical physics to excitation dynamics in nanoscale and biological systems.

■ ACKNOWLEDGMENTS

This work was supported by the National Science Foundation of China, Grant Nos. 21573022, 51861135101, 21973006, 21688102, and 21590801. R.L. acknowledges the Recruitment Program of Global Youth Experts of China, the Beijing Normal University Startup, and the Fundamental Research Funds for the Central Universities. O.V.P. acknowledges support of the U.S. National Science Foundation, Grant No. CHE-1900510, for methods development and the U.S. Department of Energy, Grant No. DE-SC0014429, for applications.

■ REFERENCES

(1) Snaith, H. J. Perovskites: The Emergence of a New Era for Low-Cost, High-Efficiency Solar Cells. *J. Phys. Chem. Lett.* **2013**, *4*, 3623−3630.
(2) Yang, J.-M.; Luo, Y.; Bao, Q.; Li, Y.-Q.; Tang, J.-X. Recent Advances in Energetics and Stability of Metal Halide Perovskites for Optoelectronic Applications. *Adv. Mater. Interfaces* **2019**, *6*, 1801351.
(3) Wu, Y.; Xie, F.; Chen, H.; Yang, X.; Su, H.; Cai, M.; Zhou, Z.; Noda, T.; Han, L. Thermally Stable $MAPbI_3$ Perovskite Solar Cells with Efficiency of 19.19% and Area over 1 cm^2 achieved by Additive Engineering. *Adv. Mater.* **2017**, *29*, 1701073.
(4) Deschler, F.; Price, M.; Pathak, S.; Klintberg, L. E.; Jarausch, D.-D.; Higler, R.; Hüttner, S.; Leijtens, T.; Stranks, S. D.; Snaith, H. J.; et al. High Photoluminescence Efficiency and Optically Pumped Lasing in Solution-Processed Mixed Halide Perovskite Semiconductors. *J. Phys. Chem. Lett.* **2014**, *5*, 1421−1426.
(5) Yang, W. S.; Noh, J. H.; Jeon, N. J.; Kim, Y. C.; Ryu, S.; Seo, J.; Seok, S. I. High-Performance Photovoltaic Perovskite Layers Fabricated Through Intramolecular Exchange. *Science* **2015**, *348*, 1234−1237.
(6) Ščajev, P.; Qin, C.; Aleksiejūnas, R. n.; Baronas, P.; Miasojedovas, S.; Fujihara, T.; Matsushima, T.; Adachi, C.; Juršėnas, S. Diffusion Enhancement in Highly Excited $MAPbI_3$ Perovskite Layers with Additives. *J. Phys. Chem. Lett.* **2018**, *9*, 3167−3172.
(7) Zhao, Y.; Nardes, A. M.; Zhu, K. Solid-State Mesostructured Perovskite $CH_3NH_3PbI_3$ Solar Cells: Charge Transport, Recombination, and Diffusion Length. *J. Phys. Chem. Lett.* **2014**, *5*, 490−494.
(8) Hutter, E. M.; Eperon, G. E.; Stranks, S. D.; Savenije, T. J. Charge Carriers in Planar and Meso-Structured Organic-Inorganic Perovskites: Mobilities, Lifetimes, and Concentrations of Trap States. *J. Phys. Chem. Lett.* **2015**, *6*, 3082−3090.
(9) Shi, D.; Adinolfi, V.; Comin, R.; Yuan, M.; Alarousu, E.; Buin, A.; Chen, Y.; Hoogland, S.; Rothenberger, A.; Katsiev, K.; et al. Low Trap-State Density and Long Carrier Diffusion in Organolead Trihalide Perovskite Single Crystals. *Science* **2015**, *347*, 519−522.
(10) Stranks, S. D.; Eperon, G. E.; Grancini, G.; Menelaou, C.; Alcocer, M. J.; Leijtens, T.; Herz, L. M.; Petrozza, A.; Snaith, H. J. Electron-Hole Diffusion Lengths Exceeding 1 Micrometer in an Organometal Trihalide Perovskite Absorber. *Science* **2013**, *342*, 341−344.
(11) Wang, X.; Ling, Y.; Chiu, Y. C.; Du, Y.; Barreda, J. L.; Perez-Orive, F.; Ma, B.; Xiong, P.; Gao, H. Dynamic Electronic Junctions in Organic-Inorganic Hybrid Perovskites. *Nano Lett.* **2017**, *17*, 4831−4839.
(12) Shang, M.-H.; Zhang, J.; Zhang, P.; Yang, Z.; Zheng, J.; Haque, M. A.; Yang, W.; Wei, S.-H.; Wu, T. Stable Bandgap-Tunable Hybrid Perovskites with Alloyed Pb-Ba Cations for High-Performance Photovoltaic Applications. *J. Phys. Chem. Lett.* **2019**, *10*, 59−66.
(13) Ogomi, Y.; Morita, A.; Tsukamoto, S.; Saitho, T.; Fujikawa, N.; Shen, Q.; Toyoda, T.; Yoshino, K.; Pandey, S. S.; Ma, T.; et al. $CH_3NH_3SnxPb_{1-x}I_3$ Perovskite Solar Cells Covering up to 1060 nm. *J. Phys. Chem. Lett.* **2014**, *5*, 1004−1011.
(14) Noh, J. H.; Im, S. H.; Heo, J. H.; Mandal, T. N.; Seok, S. I. Chemical Management for Colorful, Efficient, and Stable Inorganic-Organic Hybrid Nanostructured Solar Cells. *Nano Lett.* **2013**, *13*, 1764−1769.
(15) Abdelhady, A. L.; Saidaminov, M. I.; Murali, B.; Adinolfi, V.; Voznyy, O.; Katsiev, K.; Alarousu, E.; Comin, R.; Dursun, I.; Sinatra, L.; et al. Heterovalent Dopant Incorporation for Bandgap and Type Engineering of Perovskite Crystals. *J. Phys. Chem. Lett.* **2016**, *7*, 295−301.
(16) Gao, L.; Zeng, K.; Guo, J.; Ge, C.; Du, J.; Zhao, Y.; Chen, C.; Deng, H.; He, Y.; Song, H.; et al. Passivated Single-Crystalline $CH_3NH_3PbI_3$ Nanowire Photodetector with High Detectivity and Polarization Sensitivity. *Nano Lett.* **2016**, *16*, 7446−7454.
(17) Wong, A. B.; Lai, M.; Eaton, S. W.; Yu, Y.; Lin, E.; Dou, L.; Fu, A.; Yang, P. Growth and Anion Exchange Conversion of $CH_3NH_3PbX_3$ Nanorod Arrays for Light-Emitting Diodes. *Nano Lett.* **2015**, *15*, 5519−5524.
(18) Yantara, N.; Bhaumik, S.; Yan, F.; Sabba, D.; Dewi, H. A.; Mathews, N.; Boix, P. P.; Demir, H. V.; Mhaisalkar, S. Inorganic Halide Perovskites for Efficient Light-Emitting Diodes. *J. Phys. Chem. Lett.* **2015**, *6*, 4360−4364.
(19) Kojima, A.; Teshima, K.; Shirai, Y.; Miyasaka, T. Organometal Halide Perovskites as Visible-Light Sensitizers for Photovoltaic Cells. *J. Am. Chem. Soc.* **2009**, *131*, 6050−6051.
(20) NREL. Best Research-Cell Efficiency Chart. https://www.nrel.gov/pv/cell-efficiency.html (accessed August 5, 2019).
(21) Shockley, W.; Queisser, H. J. Detailed Balance Limit of Efficiency of P-N Junction Solar Cells. *J. Appl. Phys.* **1961**, *32*, 510−519.
(22) Jankowska, J.; Long, R.; Prezhdo, O. V. Quantum Dynamics of Photogenerated Charge Carriers in Hybrid Perovskites: Dopants, Grain Boundaries, Electric Order, and Other Realistic Aspects. *ACS Energy Lett.* **2017**, *2*, 1588−1597.
(23) Wolff, C. M.; Caprioglio, P.; Stolterfoht, M.; Neher, D. Nonradiative Recombination in Perovskite Solar Cells: The Role of Interfaces. *Adv. Mater.* **2019**, *31*, 1902762.
(24) Klimov, V. I.; Mikhailovsky, A. A.; McBranch, D. W.; Leatherdale, C. A.; Bawendi, M. G. Quantization of Multiparticle

Auger Rates in Semiconductor Quantum Dots. *Science* **2000**, *287*, 1011−1013.
(25) Luo, D.; Su, R.; Zhang, W.; Gong, Q.; Zhu, R. Minimizing Non-Radiative Recombination Losses in Perovskite Solar Cells. *Nat. Rev. Mater.* **2020**, *5*, 44−60.
(26) Bi, D.; Yi, C.; Luo, J.; Decoppet, J.-D.; Zhang, F.; Zakeeruddin, S. M.; Li, X.; Hagfeldt, A.; Gratzel, M. Polymer-Templated Nucleation and Crystal Growth of Perovskite Films for Solar Cells with Efficiency Greater than 21%. *Nat. Energy* **2016**, *1*, 16142.
(27) Sherkar, T. S.; Momblona, C.; Gil-Escrig, L.; Avila, J.; Sessolo, M.; Bolink, H. J.; Koster, L. J. A. Recombination in Perovskite Solar Cells: Significance of Grain Boundaries, Interface Traps, and Defect Ions. *ACS Energy Lett.* **2017**, *2*, 1214−1222.
(28) Chen, B.; Rudd, P. N.; Yang, S.; Yuan, Y.; Huang, J. Imperfections and Their Passivation in Halide Perovskite Solar Cells. *Chem. Soc. Rev.* **2019**, *48*, 3842−3867.
(29) Kanhere, P.; Chakraborty, S.; Rupp, C. J.; Ahuja, R.; Chen, Z. Substitution Induced Band Structure Shape Tuning in Hybrid Perovskites $CH_3NH_3Pb_{1-x}Sn_xI_3$ for Efficient Solar Cell Applications. *RSC Adv.* **2015**, *5*, 107497−107502.
(30) Zhu, H.; Miyata, K.; Fu, Y.; Wang, J.; Joshi, P. P.; Niesner, D.; Williams, K. W.; Jin, S.; Zhu, X. Y. Screening in Crystalline Liquids Protects Energetic Carriers in Hybrid Perovskites. *Science* **2016**, *353*, 1409−1413.
(31) Correa-Baena, J.-P.; Luo, Y.; Brenner, T. M.; Snaider, J.; Sun, S.; Li, X.; Jensen, M. A.; Hartono, N. T. P.; Nienhaus, L.; Wieghold, S.; et al. Homogenized Halides and Alkali Cation Segregation in Alloyed Organic-Inorganic Perovskites. *Science* **2019**, *363*, 627−631.
(32) deQuilettes, D. W.; Vorpahl, S. M.; Stranks, S. D.; Nagaoka, H.; Eperon, G. E.; Ziffer, M. E.; Snaith, H. J.; Ginger, D. S. Impact of Microstructure on Local Carrier Lifetime in Perovskite Solar Cells. *Science* **2015**, *348*, 683−686.
(33) Xiao, G.; Cao, Y.; Qi, G.; Wang, L.; Liu, C.; Ma, Z.; Yang, X.; Sui, Y.; Zheng, W.; Zou, B. Pressure Effects on Structure and Optical Properties in Cesium Lead Bromide Perovskite Nanocrystals. *J. Am. Chem. Soc.* **2017**, *139*, 10087−10094.
(34) Zhu, Z.; Ma, J.; Wang, Z.; Mu, C.; Fan, Z.; Du, L.; Bai, Y.; Fan, L.; Yan, H.; Phillips, D. L.; et al. Efficiency Enhancement of Perovskite Solar Cells through Fast Electron Extraction: The Role of Graphene Quantum Dots. *J. Am. Chem. Soc.* **2014**, *136*, 3760−3763.
(35) Bornemann, F. A.; Nettesheim, P.; Schutte, C. Quantum-Classical Molecular Dynamics as an Approximation to Full Quantum Dynamics. *J. Chem. Phys.* **1996**, *105*, 1074−1083.
(36) Jasper, A. W.; Nangia, S.; Zhu, C. Y.; Truhlar, D. G. Non-Born-Oppenheimer Molecular Dynamics. *Acc. Chem. Res.* **2006**, *39*, 101−108.
(37) Jaeger, H. M.; Fischer, S.; Prezhdo, O. V. Decoherence-Induced Surface Hopping. *J. Chem. Phys.* **2012**, *137*, 22A545.
(38) Nijjar, P.; Jankowska, J.; Prezhdo, O. V. Ehrenfest and Classical Path Dynamics with Decoherence and Detailed Balance. *J. Chem. Phys.* **2019**, *150*, 204124.
(39) Wang, L.; Akimov, A.; Prezhdo, O. V. Recent Progress in Surface Hopping: 2011−2015. *J. Phys. Chem. Lett.* **2016**, *7*, 2100−2112.
(40) Wang, L.; Sifain, A. E.; Prezhdo, O. V. Fewest Switches Surface Hopping in Liouville Space. *J. Phys. Chem. Lett.* **2015**, *6*, 3827−3833.
(41) Wang, L.; Trivedi, D.; Prezhdo, O. V. Global Flux Surface Hopping Approach for Mixed Quantum-Classical Dynamics. *J. Chem. Theory Comput.* **2014**, *10*, 3598−3605.
(42) Akimov, A. V.; Long, R.; Prezhdo, O. V. Coherence Penalty Functional: A Simple Method for Adding Decoherence in Ehrenfest Dynamics. *J. Chem. Phys.* **2014**, *140*, 194107.
(43) Brooksby, C.; Prezhdo, O. V. Quantized Mean-Field Approximation. *Chem. Phys. Lett.* **2001**, *346*, 463−469.
(44) Craig, C. F.; Duncan, W. R.; Prezhdo, O. V. Trajectory Surface Hopping in the Time-Dependent Kohn-Sham Approach for Electron-Nuclear Dynamics. *Phys. Rev. Lett.* **2005**, *95*, 163001.
(45) Akimov, A. V.; Prezhdo, O. V. Persistent Electronic Coherence Despite Rapid Loss of Electron-Nuclear Correlation. *J. Phys. Chem. Lett.* **2013**, *4*, 3857−3864.
(46) Marques, M. A. L.; Gross, E. K. U. Time-Dependent Density Functional Theory. *Annu. Rev. Phys. Chem.* **2004**, *55*, 427−455.
(47) Baer, R.; Neuhauser, D. Real-Time Linear Response for Time-Dependent Density-Functional Theory. *J. Chem. Phys.* **2004**, *121*, 9803−9807.
(48) Chernyak, V.; Mukamel, S. Density-Matrix Representation of Nonadiabatic Couplings in Time-Dependent Density Functional (TDDFT) Theories. *J. Chem. Phys.* **2000**, *112*, 3572−3579.
(49) Baer, R. Non-Adiabatic Couplings by Time-Dependent Density Functional Theory. *Chem. Phys. Lett.* **2002**, *364*, 75−79.
(50) Akimov, A. V.; Prezhdo, O. V. The PYXAID Program for Non-Adiabatic Molecular Dynamics in Condensed Matter Systems. *J. Chem. Theory Comput.* **2013**, *9*, 4959−4972.
(51) Akimov, A. V.; Prezhdo, O. V. Advanced Capabilities of the PYXAID Program: Integration Schemes, Decoherence Effects, Multiexcitonic States, and Field-Matter Interaction. *J. Chem. Theory Comput.* **2014**, *10*, 789−804.
(52) Mukamel, S. *Principles of Nonlinear Optical Spectroscopy*; Oxford University Press: New York, 1995.
(53) Kamisaka, H.; Kilina, S. V.; Yamashita, K.; Prezhdo, O. V. Ab Initio Study of Temperature and Pressure Dependence of Energy and Phonon-Induced Dephasing of Electronic Excitations in CdSe and PbSe Quantum Dots. *J. Phys. Chem. C* **2008**, *112*, 7800−7808.
(54) Lee, M. M.; Teuscher, J.; Miyasaka, T.; Murakami, T. N.; Snaith, H. J. Efficient Hybrid Solar Cells Based on Meso-Superstructured Organometal Halide Perovskites. *Science* **2012**, *338*, 643−647.
(55) Wang, Z.; Shi, Z.; Li, T.; Chen, Y.; Huang, W. Stability of Perovskite Solar Cells: A Prospective on the Substitution of the A Cation and X Anion. *Angew. Chem., Int. Ed.* **2017**, *56*, 1190−1212.
(56) Zhao, Y.; Zhu, K. Organic-Inorganic Hybrid Lead Halide Perovskites for Optoelectronic and Electronic Applications. *Chem. Soc. Rev.* **2016**, *45*, 655−689.
(57) Liu, J.; Shirai, Y.; Yang, X.; Yue, Y.; Chen, W.; Wu, Y.; Islam, A.; Han, L. High-Quality Mixed-Organic-Cation Perovskites from a Phase-Pure Non-stoichiometric Intermediate $FAI_{(1-x)}$-PbI_2 for Solar Cells. *Adv. Mater.* **2015**, *27*, 4918−4923.
(58) Kieslich, G.; Sun, S.; Cheetham, A. K. Solid-State Principles Applied to Organic-Inorganic Perovskites: New Tricks for an Old Dog. *Chem. Sci.* **2014**, *5*, 4712−4715.
(59) Giorgi, G.; Fujisawa, J.-I.; Segawa, H.; Yamashita, K. Organic-Inorganic Hybrid Lead Iodide Perovskite Featuring Zero Dipole Moment Guanidinium Cations: A Theoretical Analysis. *J. Phys. Chem. C* **2015**, *119*, 4694−4701.
(60) Makarov, N. S.; Guo, S.; Isaienko, O.; Liu, W.; Robel, I.; Klimov, V. I. Spectral and Dynamical Properties of Single Excitons, Biexcitons, and Trions in Cesium-Lead-Halide Perovskite Quantum Dots. *Nano Lett.* **2016**, *16*, 2349−2362.
(61) Wang, H.-C.; Lin, S.-Y.; Tang, A.-C.; Singh, B. P.; Tong, H.-C.; Chen, C.-Y.; Lee, Y.-C.; Tsai, T.-L.; Liu, R.-S. Mesoporous Silica Particles Integrated with All-Inorganic $CsPbBr_3$ Perovskite Quantum-Dot Nanocomposites (MP-PQDs) with High Stability and Wide Color Gamut Used for Backlight Display. *Angew. Chem., Int. Ed.* **2016**, *55*, 7924−7929.
(62) Galkowski, K.; Surrente, A.; Baranowski, M.; Zhao, B.; Yang, Z.; Sadhanala, A.; Mackowski, S.; Stranks, S. D.; Plochocka, P. Excitonic Properties of Low-Band-Gap Lead-Tin Halide Perovskites. *ACS Energy Lett.* **2019**, *4*, 615−621.
(63) Abdelmageed, G.; Jewell, L.; Hellier, K.; Seymour, L.; Luo, B.; Bridges, F.; Zhang, J. Z.; Carter, S. Mechanisms for Light Induced Degradation in $MAPbI_3$ Perovskite Thin Films and Solar Cells. *Appl. Phys. Lett.* **2016**, *109*, 233905.
(64) Yin, W.-J.; Yang, J.-H.; Kang, J.; Yan, Y.; Wei, S.-H. Halide Perovskite Materials for Solar Cells: a Theoretical Review. *J. Mater. Chem. A* **2015**, *3*, 8926−8942.

https://dx.doi.org/10.1021/acs.jpclett.0c01687
J. Phys. Chem. Lett. 2020, 11, 7066−7082

(65) Phung, N.; Felix, R.; Meggiolaro, D.; Al-Ashouri, A.; Sousa e Silva, G.; Hartmann, C.; Hidalgo, J.; Koebler, H.; Mosconi, E.; Lai, B.; et al. The Doping Mechanism of Halide Perovskite Unveiled by Alkaline Earth Metals. *J. Am. Chem. Soc.* **2020**, *142*, 2364−2374.
(66) Frolova, L. A.; Anokhin, D. V.; Gerasimov, K. L.; Dremova, N. N.; Troshin, P. A. Exploring the Effects of the Pb^{2+} Substitution in $MAPbI_3$ on the Photovoltaic Performance of the Hybrid Perovskite Solar Cells. *J. Phys. Chem. Lett.* **2016**, *7*, 4353−4357.
(67) Xiao, Z.; Yan, Y. Progress in Theoretical Study of Metal Halide Perovskite Solar Cell Materials. *Adv. Energy Mater.* **2017**, *7*, 1701136.
(68) Fu, Y.; Rea, M. T.; Chen, J.; Morrow, D. J.; Hautzinger, M. P.; Zhao, Y.; Pan, D.; Manger, L. H.; Wright, J. C.; Goldsmith, R. H.; et al. Selective Stabilization and Photophysical Properties of Metastable Perovskite Polymorphs of $CsPbI_3$ in Thin Films. *Chem. Mater.* **2017**, *29*, 8385−8394.
(69) Yettapu, G. R.; Talukdar, D.; Sarkar, S.; Swarnkar, A.; Nag, A.; Ghosh, P.; Mandal, P. Terahertz Conductivity within Colloidal $CsPbBr_3$ Perovskite Nanocrystals: Remarkably High Carrier Mobilities and Large Diffusion Lengths. *Nano Lett.* **2016**, *16*, 4838−4848.
(70) Mondal, N.; Samanta, A. Complete Ultrafast Charge Carrier Dynamics in Photo-Excited All-Inorganic Perovskite Nanocrystals $CsPbX_3$. *Nanoscale* **2017**, *9*, 1878−1885.
(71) He, J.; Fang, W.-H.; Long, R.; Prezhdo, O. V. Increased Lattice Stiffness Suppresses Nonradiative Charge Recombination in $MAPbI_3$ Doped with Larger Cations: Time Domain Ab Initio Analysis. *ACS Energy Lett.* **2018**, *3*, 2070−2076.
(72) Conings, B. D. J.; Gauquelin, N.; Babayigit, A.; D'Haen, J.; D'Olieslaeger, L.; Ethirajan, A.; Verbeeck, J.; Manca, J.; Mosconi, E.; et al. Intrinsic Thermal Instability of Methylammonium Lead Trihalide Perovskite. *Adv. Energy Mater.* **2015**, *5*, 1500477.
(73) De Marco, N. Z. H. P.; Chen, Q.; Sun, P. Y.; Liu, Z. H.; Meng, L.; Yao, E.-P.; Liu, Y. S.; Schiffer, A.; Yang, Y. Guanidinium: A Route to Enhanced Carrier Lifetime and Open-Circuit Voltage in Hybrid Perovskite Solar Cells. *Nano Lett.* **2016**, *16*, 1009−1016.
(74) Shi, R.; Long, R. Hole Localization Inhibits Charge Recombination in Tin-Lead Mixed Perovskites: Time-Domain ab Initio Analysis. *J. Phys. Chem. Lett.* **2019**, *10*, 6604−6612.
(75) He, J.; Vasenko, A. S.; Long, R.; Prezhdo, O. V. Halide Composition Controls Electron-Hole Recombination in Cesium-Lead Halide Perovskite Quantum Dots: A Time Domain Ab Initio Study. *J. Phys. Chem. Lett.* **2018**, *9*, 1872−1879.
(76) Zhu, X. Y.; Podzorov, V. Charge Carriers in Hybrid Organic-Inorganic Lead Halide Perovskites Might Be Protected as Large Polarons. *J. Phys. Chem. Lett.* **2015**, *6*, 4758−4761.
(77) Baikie, T.; Fang, Y.; Kadro, J. M.; Schreyer, M.; Wei, F.; Mhaisalkar, S. G.; Graetzel, M.; White, T. J. Synthesis and Crystal Chemistry of the Hybrid Perovskite $CH_3NH_3PbI_3$ for Solid-State Sensitised Solar Cell Applications. *J. Mater. Chem. A* **2013**, *1*, 5628−5641.
(78) Onodayamamuro, N.; Matsuo, T.; Suga, H. Calorimetric and IR Spectroscopic Studies of Phase Transitions in Methylammonium Trihalogenoplumbates. *J. Phys. Chem. Solids* **1990**, *51*, 1383−1395.
(79) Poglitsch, A.; Weber, D. Dynamic Disorder in Methylammoniumtrihalogenoplumbates Observed by Millimeter-wave Spectroscopy. *J. Chem. Phys.* **1987**, *87*, 6373−6378.
(80) Sherkar, T. S.; Koster, L. J. A. Can Ferroelectric Polarization Explain the High Performance of Hybrid Halide Perovskite Solar Cells? *Phys. Chem. Chem. Phys.* **2016**, *18*, 331−338.
(81) Ivanovska, T.; Dionigi, C.; Mosconi, E.; De Angelis, F.; Liscio, F.; Morandi, V.; Ruani, G. Long-Lived Photoinduced Polarons in Organohalide Perovskites. *J. Phys. Chem. Lett.* **2017**, *8*, 3081−3086.
(82) Rohm, H.; Leonhard, T.; Schulz, A. D.; Wagner, S.; Hoffmann, M. J.; Colsmann, A. Ferroelectric Properties of Perovskite Thin Films and Their Implications for Solar Energy Conversion. *Adv. Mater.* **2019**, *31*, 1806661.
(83) Qiao, L.; Fang, W.-H.; Long, R. Ferroelectric Polarization Suppresses Nonradiative Electron-Hole Recombination in $CH_3NH_3PbI_3$ Perovskites: A Time-Domain ab Initio Study. *J. Phys. Chem. Lett.* **2019**, *10*, 7237−7244.
(84) Walsh, A. Principles of Chemical Bonding and Band Gap Engineering in Hybrid Organic-Inorganic Halide Perovskites. *J. Phys. Chem. C* **2015**, *119*, 5755−5760.
(85) Wasylishen, R. E.; Knop, O.; Macdonald, J. B. Cation Rotation in Methylammonium Lead Halides. *Solid State Commun.* **1985**, *56*, 581−582.
(86) Ma, J.; Wang, L.-W. Nanoscale Charge Localization Induced by Random Orientations of Organic Molecules in Hybrid Perovskite $CH_3NH_3PbI_3$. *Nano Lett.* **2015**, *15*, 248−253.
(87) Zhang, Z.; Long, R.; Tokina, M. V.; Prezhdo, O. V. Interplay between Localized and Free Charge Carriers Can Explain Hot Fluorescence in the $CH_3NH_3PbBr_3$ Perovskite: Time-Domain Ab Initio Analysis. *J. Am. Chem. Soc.* **2017**, *139*, 17327−17333.
(88) Miyata, K.; Meggiolaro, D.; Trinh, M. T.; Joshi, P. P.; Mosconi, E.; Jones, S. C.; De Angelis, F.; Zhu, X. Y. Large Polarons in Lead Halide Perovskites. *Sci. Adv.* **2017**, *3*, No. e1701217.
(89) Santomauro, F. G. G. J.; Mewes, L.; Nedelcu, G.; Yakunin, S.; Rossi, T.; Capano, G.; Al Haddad, A.; Budarz, J.; Kinschel, D.; et al. Localized Holes and Delocalized Electrons in Photoexcited Inorganic Perovskites: Watching Each Atomic Actor by Picosecond X-Ray Absorption Spectroscopy. *Struct. Dyn.* **2017**, *4*, 044002.
(90) He, J.; Guo, M.; Long, R. Photoinduced Localized Hole Delays Nonradiative Electron-Hole Recombination in Cesium-Lead Halide Perovskites: A Time-Domain Ab Initio Analysis. *J. Phys. Chem. Lett.* **2018**, *9*, 3021−3028.
(91) Jeon, N. J.; Noh, J. H.; Yang, W. S.; Kim, Y. C.; Ryu, S.; Seo, J.; Seok, S. I. Compositional Engineering of Perovskite Materials for High-Performance Solar Cells. *Nature* **2015**, *517*, 476−480.
(92) Jin, H.; Debroye, E.; Keshavarz, M.; Scheblykin, I. G.; Roeffaers, M. B. J.; Hofkens, J.; Steele, J. A. It's a Trap! On the Nature of Localised States and Charge Trapping in Lead Halide Perovskites. *Mater. Horiz.* **2020**, *7*, 397−410.
(93) Ono, L. K.; Liu, S.; Qi, Y. Reducing Detrimental Defects for High-Performance Metal Halide Perovskite Solar Cells. *Angew. Chem., Int. Ed.* **2020**, *59*, 6676−6698.
(94) Shao, Y.; Xiao, Z.; Bi, C.; Yuan, Y.; Huang, J. Origin and Elimination of Photocurrent Hysteresis by Fullerene Passivation in $CH_3NH_3PbI_3$ Planar Heterojunction Solar Cells. *Nat. Commun.* **2014**, *5*, 5784.
(95) Noel, N. K.; Abate, A.; Stranks, S. D.; Parrott, E. S.; Burlakov, V. M.; Goriely, A.; Snaith, H. J. Enhanced Photoluminescence and Solar Cell Performance via Lewis Base Passivation of Organic Inorganic Lead Halide Perovskites. *ACS Nano* **2014**, *8*, 9815−9821.
(96) Qin, P.-L.; Yang, G.; Ren, Z.-w.; Cheung, S. H.; So, S. K.; Chen, L.; Hao, J.; Hou, J.; Li, G. Stable and Efficient Organo-Metal Halide Hybrid Perovskite Solar Cells via π-Conjugated Lewis Base Polymer Induced Trap Passivation and Charge Extraction. *Adv. Mater.* **2018**, *30*, 1706126.
(97) Saliba, M.; Matsui, T.; Domanski, K.; Seo, J.-Y.; Ummadisingu, A.; Zakeeruddin, S. M.; Correa-Baena, J.-P.; Tress, W. R.; Abate, A.; Hagfeldt, A.; et al. Incorporation of Rubidium Cations into Perovskite Solar Cells Improves Photovoltaic Performance. *Science* **2016**, *354*, 206−209.
(98) Turren-Cruz, S.-H.; Saliba, M.; Mayer, M. T.; Juarez-Santiesteban, H.; Mathew, X.; Nienhaus, L.; Tress, W.; Erodici, M. P.; Sher, M.-J.; Bawendi, M. G.; et al. Enhanced Charge Carrier Mobility and Lifetime Suppress Hysteresis and Improve Efficiency in Planar Perovskite Solar Cells. *Energy Environ. Sci.* **2018**, *11*, 78−86.
(99) Lu, D.; Zhang, Y.; Lai, M.; Lee, A.; Xie, C.; Lin, J.; Lei, T.; Lin, Z.; Kley, C. S.; Huang, J.; et al. Giant Light-Emission Enhancement in Lead Halide Perovskites by Surface Oxygen Passivation. *Nano Lett.* **2018**, *18*, 6967−6973.
(100) Solanki, A.; Lim, S. S.; Mhaisalkar, S.; Sum, T. C. Role of Water in Suppressing Recombination Pathways in $CH_3NH_3PbI_3$ Perovskite Solar Cells. *ACS Appl. Mater. Interfaces* **2019**, *11*, 25474−25482.
(101) Jung, M.; Shin, T. J.; Seo, J.; Kim, G.; Seok, S. I. Structural Features and Their Functions in Surfactant-Armoured Methylammo-

nium Lead Iodide Perovskites for Highly Efficient and Stable Solar Cells. *Energy Environ. Sci.* **2018**, *11*, 2188−2197.
(102) Tong, C.-J.; Geng, W.; Prezhdo, O. V.; Liu, L.-M. Role of Methylammonium Orientation in Ion Diffusion and Current Voltage Hysteresis in the $CH_3NH_3PbI_3$ Perovskite. *ACS Energy Lett.* **2017**, *2*, 1997−2004.
(103) Yang, W. S.; Park, B.-W.; Jung, E. H.; Jeon, N. J.; Kim, Y. C.; Lee, D. U.; Shin, S. S.; Seo, J.; Kim, E. K.; Noh, J. H.; et al. Iodide Management in Formamidinium-Lead-Halide-Based Perovskite Layers for Efficient Solar Cells. *Science* **2017**, *356*, 1376−1379.
(104) Wang, S.; Jiang, Y.; Juarez-Perez, E. J.; Ono, L. K.; Qi, Y. Accelerated Degradation of Methylammonium Lead Iodide Perovskites Induced by Exposure to Iodine Vapour. *Nat. Energy* **2017**, *2*, 16195.
(105) He, J.; Fang, W.-h.; Long, R. Unravelling the Effects of Oxidation State of Interstitial Iodine and Oxygen Passivation on Charge Trapping and Recombination in $CH_3NH_3PbI_3$ Perovskite: a Time-Domain Ab Initio Study. *Chem. Sci.* **2019**, *10*, 10079−10088.
(106) Meggiolaro, D.; De Angelis, F. First-Principles Modeling of Defects in Lead Halide Perovskites: Best Practices and Open Issues. *ACS Energy Lett.* **2018**, *3*, 2206−2222.
(107) Tian, Y.; Peter, M.; Unger, E.; Abdellah, M.; Zheng, K.; Pullerits, T.; Yartsev, A.; Sundstrom, V.; Scheblykin, I. G. Mechanistic Insights into Perovskite Photoluminescence Enhancement: Light Curing with Oxygen Can Boost Yield Thousandfold. *Phys. Chem. Chem. Phys.* **2015**, *17*, 24978−24987.
(108) Brenes, R.; Eames, C.; Bulovic, V.; Islam, M. S.; Stranks, S. D. The Impact of Atmosphere on the Local Luminescence Properties of Metal Halide Perovskite Grains. *Adv. Mater.* **2018**, *30*, 1706208.
(109) He, J.; Fang, W.-H.; Long, R.; Prezhdo, O. V. Superoxide/Peroxide Chemistry Extends Charge Carriers' Lifetime but Undermines Chemical Stability of $CH_3NH_3PbI_3$ Exposed to Oxygen: Time-Domain ab Initio Analysis. *J. Am. Chem. Soc.* **2019**, *141*, 5798−5807.
(110) Qiao, L.; Long, R.; Fang, W.-H. Surface Pb-Dimer Passivated by Molecule Oxygen Notably Suppresses Charge Recombination in $CsPbBr_3$ Perovskites: Time-Domain Ab Initio Analysis. *J. Phys. Chem. Lett.* **2019**, *10*, 5499−5506.
(111) Fang, Z.; He, H.; Gan, L.; Li, J.; Ye, Z. Understanding the Role of Lithium Doping in Reducing Nonradiative Loss in Lead Halide Perovskites. *Adv. Sci.* **2018**, *5*, 1800736.
(112) Zhao, W.; Yao, Z.; Yu, F.; Yang, D.; Liu, S. Alkali Metal Doping for Improved $CH_3NH_3PbI_3$ Perovskite Solar Cells. *Adv. Sci.* **2018**, *5*, 1700131.
(113) Mosconi, E.; Meggiolaro, D.; Snaith, H. J.; Stranks, S. D.; De Angelis, F. Light-Induced Annihilation of Frenkel Defects in Organo-Lead Halide Perovskites. *Energy Environ. Sci.* **2016**, *9*, 3180−3187.
(114) Qiao, L.; Fang, W.-H.; Long, R.; Prezhdo, O. V. Extending Carrier Lifetimes in Lead Halide Perovskites with Alkali Metals by Passivating and Eliminating Halide Interstitial Defects. *Angew. Chem., Int. Ed.* **2020**, *59*, 4684.
(115) Song, Z.; Watthage, S. C.; Phillips, A. B.; Tompkins, B. L.; Ellingson, R. J.; Heben, M. J. Impact of Processing Temperature and Composition on the Formation of Methylammonium Lead Iodide Perovskites. *Chem. Mater.* **2015**, *27*, 4612−4619.
(116) Nie, W.; Tsai, H.; Asadpour, R.; Blancon, J.-C.; Neukirch, A. J.; Gupta, G.; Crochet, J. J.; Chhowalla, M.; Tretiak, S.; Alam, M. A.; et al. High-efficiency Solution-Processed Perovskite Solar Cells with Millimeter-Scale Grains. *Science* **2015**, *347*, 522−525.
(117) Chu, Z.; Yang, M.; Schulz, P.; Wu, D.; Ma, X.; Seifert, E.; Sun, L.; Li, X.; Zhu, K.; Lai, K. Impact of Grain Boundaries on Efficiency and Stability of Organic-Inorganic Trihalide Perovskites. *Nat. Commun.* **2017**, *8*, 2230.
(118) Long, R.; Liu, J.; Prezhdo, O. V. Unravelling the Effects of Grain Boundary and Chemical Doping on Electron-Hole Recombination in $CH_3NH_3PbI_3$ Perovskite by Time-Domain Atomistic Simulation. *J. Am. Chem. Soc.* **2016**, *138*, 3884−3890.
(119) Wang, Y.; Fang, W.-H.; Long, R.; Prezhdo, O. V. Symmetry Breaking at $MAPbI_3$ Perovskite Grain Boundaries Suppresses Charge Recombination: Time-Domain ab Initio Analysis. *J. Phys. Chem. Lett.* **2019**, *10*, 1617−1623.
(120) Wang, Y.; He, J.; Yang, Y.; Zhang, Z.; Long, R. Chlorine Passivation of Grain Boundary Suppresses Electron-Hole Recombination in $CsPbBr_3$ Perovskite by Nonadiabatic Molecular Dynamics Simulation. *ACS Appl. Energy Mater.* **2019**, *2*, 3419−3426.
(121) Deschler, F.; Price, M.; Pathak, S.; Klintberg, L. E.; Jarausch, D.-D.; Higler, R.; Huettner, S.; Leijtens, T.; Stranks, S. D.; Snaith, H. J.; et al. High Photoluminescence Efficiency and Optically Pumped Lasing in Solution-Processed Mixed Halide Perovskite Semiconductors. *J. Phys. Chem. Lett.* **2014**, *5*, 1421−1426.
(122) Savenije, T. J.; Ponseca, C. S., Jr.; Kunneman, L.; Abdellah, M.; Zheng, K.; Tian, Y.; Zhu, Q.; Canton, S. E.; Scheblykin, I. G.; Pullerits, T.; et al. Thermally Activated Exciton Dissociation and Recombination Control the Carrier Dynamics in Organometal Halide Perovskite. *J. Phys. Chem. Lett.* **2014**, *5*, 2189−2194.
(123) Long, R.; Fang, W.; Prezhdo, O. V. Moderate Humidity Delays Electron-Hole Recombination in Hybrid Organic-Inorganic Perovskites: Time-Domain Ab Initio Simulations Rationalize Experiments. *J. Phys. Chem. Lett.* **2016**, *7*, 3215−3222.
(124) Li, W.; Long, R.; Tang, J.; Prezhdo, O. V. Influence of Defects on Excited-State Dynamics in Lead Halide Perovskites: Time-Domain ab Initio Studies. *J. Phys. Chem. Lett.* **2019**, *10*, 3788−3804.
(125) Munson, K. T.; Kennehan, E. R.; Doucette, G. S.; Asbury, J. B. Dynamic Disorder Dominates Delocalization, Transport, and Recombination in Halide Perovskites. *Chem.* **2018**, *4*, 2826−2843.
(126) Wang, Y.; Long, R. Anomalous Temperature-Dependent Charge Recombination in $CH_3NH_3PbI_3$ Perovskite: Key Roles of Charge Localization and Thermal Effect. *ACS Appl. Mater. Interfaces* **2019**, *11*, 32069−32075.
(127) Liu, G.; Kong, L.; Yang, W.; Mao, H.-k. Pressure Engineering of Photovoltaic Perovskites. *Mater. Today* **2019**, *27*, 91−106.
(128) Kong, L.; Liu, G.; Gong, J.; Hu, Q.; Schaller, R. D.; Dera, P.; Zhang, D.; Liu, Z.; Yang, W.; Zhu, K.; et al. Simultaneous Band-Gap Narrowing and Carrier-Lifetime Prolongation of Organic-Inorganic Trihalide Perovskites. *Proc. Natl. Acad. Sci. U. S. A.* **2016**, *113*, 8910−8915.
(129) Zhang, L.; Zeng, Q.; Wang, K. Pressure-Induced Structural and Optical Properties of Inorganic Halide Perovskite $CsPbBr_3$. *J. Phys. Chem. Lett.* **2017**, *8*, 3752−3758.
(130) Wang, Y.; Long, R. Unravelling the Effects of Pressure-Induced Suppressed Electron-Hole Recombination in $CsPbBr_3$ Perovskite: Time-Domain ab Initio Analysis. *J. Phys. Chem. Lett.* **2019**, *10*, 4354−4361.
(131) Li, W.; Chen, Z.; Tang, J.; Prezhdo, O. V. Anti-correlation between Band gap and Carrier Lifetime in Lead Halide Perovskites under Compression Rationalized by Ab Initio Quantum Dynamics. *Chem. Mater.* **2020**, *32*, 4707.
(132) Lindblad, R.; Bi, D.; Park, B.-w.; Oscarsson, J.; Gorgoi, M.; Siegbahn, H.; Odelius, M.; Johansson, E. M. J.; Rensmo, H. Electronic Structure of $TiO_2/CH_3NH_3PbI_3$ Perovskite Solar Cell Interfaces. *J. Phys. Chem. Lett.* **2014**, *5*, 648−653.
(133) Mei, A.; Li, X.; Liu, L.; Ku, Z.; Liu, T.; Rong, Y.; Xu, M.; Hu, M.; Chen, J.; Yang, Y.; et al. A Hole-Conductor-Free, Fully Printable Mesoscopic Perovskite Solar Cell With High Stability. *Science* **2014**, *345*, 295−298.
(134) Wang, K.-C.; Jeng, J.-Y.; Shen, P.-S.; Chang, Y.-C.; Diau, E. W.-G.; Tsai, C.-H.; Chao, T.-Y.; Hsu, H.-C.; Lin, P.-Y.; Chen, P.; et al. P-Type Mesoscopic Nickel Oxide-Organometallic Perovskite Heterojunction Solar Cells. *Sci. Rep.* **2015**, *4*, 4756.
(135) Chen, H.; Wei, Q.; Saidaminov, M. I.; Wang, F.; Johnston, A.; Hou, Y.; Peng, Z.; Xu, K.; Zhou, W.; Liu, Z.; et al. Efficient and Stable Inverted Perovskite Solar Cells Incorporating Secondary Amines. *Adv. Mater.* **2019**, *31*, 1903559.
(136) Piatkowski, P.; Cohen, B.; Ramos, F. J.; Di Nunzio, M.; Nazeeruddin, M. K.; Graetzel, M.; Ahmad, S.; Douhal, A. Direct Monitoring of Ultrafast Electron and Hole Dynamics in Perovskite Solar Cells. *Phys. Chem. Chem. Phys.* **2015**, *17*, 14674−14684.

https://dx.doi.org/10.1021/acs.jpclett.0c01687
J. Phys. Chem. Lett. 2020, 11, 7066−7082

(137) Long, R.; Fang, W.-H.; Prezhdo, O. V. Strong Interaction at the Perovskite/TiO_2 Interface Facilitates Ultrafast Photoinduced Charge Separation: A Nonadiabatic Molecular Dynamics Study. *J. Phys. Chem. C* **2017**, *121*, 3797−3806.
(138) Long, R.; Prezhdo, O. V. Dopants Control Electron-Hole Recombination at Perovskite-TiO_2 Interfaces: Ab Initio Time-Domain Study. *ACS Nano* **2015**, *9*, 11143−11155.
(139) Shi, R.; Zhang, Z.; Fang, W.-H.; Long, R. Charge Localization Control of Electron-Hole Recombination in Multilayer Two-Dimensional Dion-Jacobson Hybrid Perovskites. *J. Mater. Chem. A* **2020**, *8*, 9168−9176.
(140) Tsai, H.; Nie, W.; Blancon, J.-C.; Stoumpos, C. C. S.; Asadpour, R.; Harutyunyan, B.; Neukirch, A. J.; Verduzco, R.; Crochet, J. J.; Tretiak, S.; et al. High-efficiency Two-Dimensional Ruddlesden-Popper Perovskite Solar Cells. *Nature* **2016**, *536*, 312−316.
(141) Blancon, J. C.; Stier, A. V.; Tsai, H.; Nie, W.; Stoumpos, C. C.; Traore, B.; Pedesseau, L.; Kepenekian, M.; Katsutani, F.; Noe, G. T.; et al. Scaling Law for Excitons in 2D Perovskite Quantum Wells. *Nat. Commun.* **2018**, *9*, 2254.
(142) Peng, W.; Yin, J.; Ho, K.-T.; Ouellette, O.; De Bastiani, M.; Murali, B.; El Tall, O.; Shen, C.; Miao, X.; Pan, J.; et al. Ultralow Self-Doping in Two-dimensional Hybrid Perovskite Single Crystals. *Nano Lett.* **2017**, *17*, 4759−4767.
(143) Mousdis, G. A.; Papavassiliou, G. C.; Raptopoulou, C. P.; Terzis, A. Preparation and Characterization of $H_3N(CH_2)_6NH_3PbI_4$ and Similar Compounds with a layered Perovskite Structure. *J. Mater. Chem.* **2000**, *10*, 515−518.
(144) Cao, D. H.; Stoumpos, C. C.; Farha, O. K.; Hupp, J. T.; Kanatzidis, M. G. 2D Homologous Perovskites as Light-Absorbing Materials for Solar Cell Applications. *J. Am. Chem. Soc.* **2015**, *137*, 7843−7850.
(145) Lin, Y.; Bai, Y.; Fang, Y.; Wang, Q.; Deng, Y.; Huang, J. Suppressed Ion Migration in Low-Dimensional Perovskites. *ACS Energy Lett.* **2017**, *2*, 1571−1572.
(146) Guo, Z.; Wu, X.; Zhu, T.; Zhu, X.; Huang, L. Electron-Phonon Scattering in Atomically Thin 2D Perovskites. *ACS Nano* **2016**, *10*, 9992−9998.
(147) Zhang, Z.; Fang, W.-H.; Tokina, M. V.; Long, R.; Prezhdo, O. V. Rapid Decoherence Suppresses Charge Recombination in Multi-Layer 2D Halide Perovskites: Time-Domain Ab Initio Analysis. *Nano Lett.* **2018**, *18*, 2459−2466.
(148) Blancon, J. C.; Tsai, H.; Nie, W.; Stoumpos, C. C.; Pedesseau, L.; Katan, C.; Kepenekian, M.; Soe, C. M. M.; Appavoo, K.; Sfeir, M. Y.; et al. Extremely Efficient Internal Exciton Dissociation Through Edge States in Layered 2D Perovskites. *Science* **2017**, *355*, 1288−1291.
(149) Zhang, Z.; Fang, W.-H.; Long, R.; Prezhdo, O. V. Exciton Dissociation and Suppressed Charge Recombination at 2D Perovskite Edges: Key Roles of Unsaturated Halide Bonds and Thermal Disorder. *J. Am. Chem. Soc.* **2019**, *141*, 15557−15566.
(150) Ahmad, S.; Fu, P.; Yu, S.; Yang, Q.; Liu, X.; Wang, X.; Wang, X.; Guo, X.; Li, C. Dion-Jacobson Phase 2D Layered Perovskites for Solar Cells with Ultrahigh Stability. *Joule* **2019**, *3*, 889−890.
(151) Cohen, B.-E.; Li, Y.; Meng, Q.; Etgar, L. Dion-Jacobson Two-Dimensional Perovskite Solar Cells Based on Benzene Dimethanammonium Cation. *Nano Lett.* **2019**, *19*, 2588−2597.
(152) Niu, T.; Ren, H.; Wu, B.; Xia, Y.; Xie, X.; Yang, Y.; Gao, X.; Chen, Y.; Huang, W. Reduced-Dimensional Perovskite Enabled by Organic Diamine for Efficient Photovoltaics. *J. Phys. Chem. Lett.* **2019**, *10*, 2349−2356.
(153) Ke, W.; Mao, L.; Stoumpos, C. C.; Hoffman, J.; Spanopoulos, I.; Mohite, A. D.; Kanatzidis, M. G. Compositional and Solvent Engineering in Dion-Jacobson 2D Perovskites Boosts Solar Cell Efficiency and Stability. *Adv. Energy Mater.* **2019**, *9*, 1803384.
(154) Aristidou, N.; Sanchez-Molina, I.; Chotchuangchutchaval, T.; Brown, M.; Martinez, L.; Rath, T.; Haque, S. A. The Role of Oxygen in the Degradation of Methylammonium Lead Trihalide Perovskite Photoactive Layers. *Angew. Chem., Int. Ed.* **2015**, *54*, 8208−8212.
(155) Milot, R. L.; Eperon, G. E.; Snaith, H. J.; Johnston, M. B.; Herz, L. M. Temperature-Dependent Charge-Carrier Dynamics in $CH_3NH_3PbI_3$ Perovskite Thin Films. *Adv. Funct. Mater.* **2015**, *25*, 6218−6227.
(156) Hutter, E. M.; Gelvez-Rueda, M. C.; Osherov, A.; Bulovic, V.; Grozema, F. C.; Stranks, S. D.; Savenije, T. J. Direct-Indirect Character of the Bandgap in Methylammonium Lead Iodide Perovskite. *Nat. Mater.* **2017**, *16*, 115−120.
(157) Li, L.; Lin, M.-F.; Zhang, X.; Britz, A.; Krishnamoorthy, A.; Ma, R.; Kalia, R. K.; Nakano, A.; Vashishta, P.; Ajayan, P.; et al. Phonon-Suppressed Auger Scattering of Charge Carriers in Defective Two-Dimensional Transition Metal Dichalcogenides. *Nano Lett.* **2019**, *19*, 6078−6086.
(158) Pal, S.; Trivedi, D. J.; Akimov, A. V.; Aradi, B.; Frauenheim, T.; Prezhdo, O. V. Nonadiabatic Molecular Dynamics for Thousand Atom Systems: A Tight-Binding Approach toward PYXAID. *J. Chem. Theory Comput.* **2016**, *12*, 1436−1448.
(159) Chen, W.-K.; Liu, X.-Y.; Fang, W.-H.; Dral, P. O.; Cui, G. Deep Learning for Nonadiabatic Excited-State Dynamics. *J. Phys. Chem. Lett.* **2018**, *9*, 6702−6708.
(160) Zhou, G.; Chu, W.; Prezhdo, O. V. Structural Deformation Controls Charge Losses in $MAPbI_3$: Unsupervised Machine Learning of Nonadiabatic Molecular Dynamics. *ACS Energy Lett.* **2020**, *5*, 1930−1938.

https://dx.doi.org/10.1021/acs.jpclett.0c01687
J. Phys. Chem. Lett. 2020, 11, 7066−7082